EXPLORING THE USE OF AN ECHO STATE NETWORK IN MODELING TURBULENT JET BEHAVIOR

by

PRADEEP SAPKOTA

JOHN BAKER, COMMITTEE CHAIR
GARY CHENG
SEMIH OLCMEN
MUHAMMAD ALI ROB SHARIF
DANIEL FONSECA

A DISSERTATION

Submitted in partial fulfillment of the requirements
for the degree of Doctor of Philosophy
in the Department of Aerospace Engineering and Mechanics
in the Graduate School of
The University of Alabama

TUSCALOOSA, ALABAMA

2021

ABSTRACT

This work investigates the use of an Echo State Network (ESN) to predict turbulent jet flow behavior. ESNs are a particular class of Recurrent Neural Networks (RNNs) that have been shown to model transient chaotic systems while avoiding some of the difficulties associated with training other types of recurrent neural networks. It is a large, random, fixed recurrent neural network in which each neuron receives a non-linear input signal, and the weights of the input and hidden neurons are fixed randomly. An extensive literature review is performed regarding the history of turbulent jet modeling and the use of an ESN to model turbulent flow analogs.

In an initial investigation, a turbulent free jet issuing from a circular tube into a quiescent medium was modeled using an ESN. ESN training was achieved using a validated LES dataset obtained from commercially available CFD software. A separate LES dataset was used to evaluate how well the ESN predicted flow field behavior. A hyperparameter search was undertaken to enhance the ESN's ability to model the turbulent flow field under consideration. The ESN model proved capable of reproducing instantaneous vortical structures and centerline velocity behavior relative to LES model data and previously published experimental data.

In a second investigation, two cases of heated turbulent jets discharging from a nozzle to a cold surrounding were studied using an ESN. LES of the jets were carried out in commercial CFD software, and the data obtained from LES were used for training and testing the ESN. Detailed comparisons of the mean velocity profiles and the mean temperature profiles along the streamwise and radial directions were provided, along with turbulence quantities. ESN showed a good agreement with LES simulation and the experiment data. The coherent structure of the jet was investigated by the visualization of

the isosurface of the Q criterion. ESN was shown to be efficient in capturing the vortex rings at the vicinity of the nozzle. The ESN also proved capable of capturing mean turbulent kinetic energy distribution for different temperature gradient values.

In the third and final investigation, the model problem was a variable density jet originating from a cylindrical tube that passed through a weakly restricted co-flow of low-speed air streams. ESN training and testing were carried out with the help of a validated LES dataset obtained from commercial CFD software. Compared to LES model data and previously published experimental data, the ESN model was able to reproduce turbulent flow field statistics. The ESN model correctly reproduced the profile shapes of radial shear stresses. The vortical evolution for the Helium jet was studied with the ESN model, and the ESN model captured the vortex rings formed at the jet exit and the large-scale structures downstream of the jet.

Based on the study, it was concluded that the ESN model has the potential to model turbulent flow fields effectively.

DEDICATION

To my parents, whose unwavering love and support have enriched my spirit, and to my brother and sister, who have taught me that if you want something bad enough, you can make it happen.

LIST OF ABBREVIATIONS AND SYMBOLS

AI	Artificial Intelligence
α	Leaking rate
β	Ridge Regression coefficient
χ	Sparsity matrix
DNS	Direct Numerical Simulation
ESN	Echo State Network
Fr	Froude Number
LES	Large Eddy Simulation
μ	molecular viscosity
N	Number of reservoir dimensions
ν	kinematic viscosity
RANS	Reynolds Average Navier Stokes Equation
Re	Reynolds number
ρ	Density
$\rho(W)$	spectral radius
RNN	Recurrent Neural Network
St	Strouhal number

ACKNOWLEDGMENTS

I want to convey my heartfelt gratitude and appreciation to Dr. John Baker, my Ph.D. advisor, for his assistance and counsel during my education. This dissertation would not have been feasible without his fantastic guidance and constant support.

I would also like to thank my committee members, Dr. Gary Cheng, Dr. Semih Olcmen, Dr. Muhammad Sharif, and Dr. Daniel Fonseca, for their guidance and support.

I want to express my gratitude to my colleague Soham Gupta for his unwavering support and advice during my Ph.D. journey.

I'd also want to express my gratitude to my friends for sticking with me for the last six years. They've been my listeners, party guests, traveling companions, and video gaming partners. Spending time with them has been and will continue to be some of the most memorable moments of my life.

I would also like to thank the Department of Aerospace Engineering and Mechanics for providing me with Teaching Assistantship throughout my time here at the University of Alabama.

Last but not least, I want to express my gratitude to my mother, father, brother, and sister. My parents have always supported, cared for, and loved me unconditionally. Without them, I would not have gotten this far. I'll always adore them.

CONTENTS

LIST OF TABLES

LIST OF FIGURES

CHAPTER 1

INTRODUCTION

1.1 Background

Turbulent flows often occur in natural and industrial systems, necessitating a detailed study. Turbulence has a significant effect on a range of phenomena associated with environmental and biological systems. The prediction of turbulent flow is crucial in the design of technical devices. However, turbulent flow is highly chaotic, three-dimensional, and unsteady. Turbulent flows consist of various scales ranging from the largest integral scales to the smallest Kolmogorov scales. Most of the kinetic energy is contained in the largest scales. Through an inertial process, this energy is cascaded to the smallest scales beyond which viscous dissipation of kinetic energy into heat results in a variety of time and length scales that must be modeled to predict turbulent flows accurately. As a result, the computing expense of modeling turbulent flows limits the realistic prediction of flow properties. Given the importance of turbulent flow prediction, much research has been done to simulate them effectively.

Historically, turbulence models such as Direct Numerical Simulation (DNS), Large Eddy Simulation (LES), and Reynolds-Averaged Navier-Stokes (RANS) have been used to simulate turbulent flows. RANS equations decompose an instantaneous variable into its time-averaged and fluctuating components using time-averaged fluid flow equations. This averaging technique adds additional terms into the equation known as Reynolds stresses, which must be modeled. In the past, many turbulence models were employed to create a closed system of equations. The physical condition of the problem often limits the application of these models. Furthermore, the modeling assumptions provided in the model's

mathematical formulation often limit RANS models. The use of RANS modeling in industrial applications was addressed in Yusuf et al. [103]. The use of RANS coupled with LES to tackle complicated flow problems was discussed in Speziale [88]. Xiao and Cinnella [100] reviewed parametric and structural uncertainties in turbulence models. Also presented was a review of the uncertainties encountered with approaches such as LES. In competition with large-eddy simulations, Hanjalic [43] offered a view of recent advances and a viewpoint on the future role of the RANS method in the computation of turbulent flows and heat transfer. Durbin [33] provided a brief review on RANS, discussing the relation between practice and theory. Wilcox [98] discussed the evolution and use of various $k - \omega$ models and its comparison to the $k - \epsilon$ model. The LES method employs a filtering process to efficiently separate the larger and smaller eddies. The larger eddies may be resolved directly, whereas the smaller, isotropic eddies should be represented using sub-grid size models. While LES modeling increases the solution's possible applicability and fidelity, it comes at a greater computational cost due to the time step requirements and higher mesh resolutions. The sub-grid scale models' uncertainties for certain flow problems also restrict their use. Zhiyin [107] provides a comprehensive overview of the use of LES for turbulent flows. Chaouat [20] provided a brief overview about the application of the combined RANS/LES technique for solving turbulent flows. The Navier-Stokes equations are solved directly in DNS, with no assumptions about models. It involves resolving various temporal and spatial scales associated with a turbulent flow, from extremely large to Kolmogorov length scales. Moin and Mahesh [67] addressed the uses and difficulties of DNS. Deen et al. [29] discussed different DNS models for gas-solid flows. Although DNS is the most accurate method of simulating turbulent flows, its applicability to industrial engineering flows is limited due to mesh size and time step limitations. As a result, it's only used to solve basic geometries and assist in comprehending turbulent flows.

The circular jet is a fluid flow phenomenon observed in many engineering fields such as fuel/oxidizer injectors, thermal management technologies, industrial smokestacks, etc. The

essential features of a turbulent jet, such as mixing and noise generation, are closely associated with the development of turbulence generated by shearing flows. Hence a precise understanding and modeling of jet flow are of real interest. The jet inflow conditions play a critical role in characterizing the development of turbulent jets extending from the evolution of initial shear layer [13, 64], to the mixing and noise generation [11, 64]. The effect of jet inflow conditions such as the jet momentum thickness was first investigated by Hussain and Zedan [45] where they found out that the distance to attain self-preservation depends both upon the initial disturbance level and the jet momentum thickness. Gutmark and Ho [40] outlined that the jet-preferred mode or the formation of coherent structures is related to the shear layer development characterized by the jet inflow conditions. Russ and Strykowski [82] studied the effect of jet momentum thickness on jet mixing at Reynold's number of $Re_D = (U_j \mathrm{D}/\nu\ )$=$10^4$, where ν is the dynamic viscosity of the fluid. They found that the centerline velocity decays slowly at a smaller jet momentum thickness value. Thus less mixing occurs. Stanley and Sarkar [90] used a direct numerical simulation of a planar jet to study the effect of jet inflow conditions and reported that the jet half-width and entrainment increases as the jet momentum thickness decreases. Bogey and Bailly [11] used Large Eddy Simulation (LES) to study jet inflow condition effects at a Reynolds number of Re_D=4×10^5. The paper by Kim and Choi [52] studied the effects of jet inflow conditions on jet flow characteristics using Large Eddy Simulation (LES). They found out that the jet characteristics significantly depend upon jet momentum thickness and Reynolds number.

Variable density turbulent flows, which may be due to temperature variations stemming from reactions or variations in the composition by fluids of different densities, exist widely in nature and technical devices. The ability to predict the turbulent mixing in flows with variable density is vital for modeling the dynamics of such flows and a prerequisite for predicting turbulent combustion situations. Unlike the extensively studied jets with constant density, variable-density jets are less well understood. Incompressible jets have been exten-

sively studied, experimentally, and numerically over the past years [21]. Very few experiments have been reported for variable density jets. An experiment where air/helium mixture was discharged into a swirling flow was carried out by Ahmed et al. [1]. Experiments on round jets of different densities obtained by premixing helium and air were studied by Sreenivasan et al. [89] and Kyle and Sreenivasan [54]. Further experiments of entrainment and mixing in transitional jets where different densities were obtained by heating the air were performed by Monkewitz et al. [69] and Monkewitz and Pfizenmaier [70]. Panchapakesan and Lumley [72] experimented by injecting helium from a round jet into open quiescent air. Experiments of helium, air, and carbon dioxide exiting into low-speed air co-flow were studied by Djeridane et al. [31], Amielh et al. [2] and more recently by Boujemaa et al. [12]. Few numerical studies have been conducted to study variable-density jets. Using Reynolds stress turbulence model Jester-Zurker et al. [49] performed a numerical analysis of non-reactive combustor flow. The agreement between numerical analysis and experiment was less satisfactory for variable-density jets. Large Eddy Simulation of round jets were performed by Zhou et al. [108], Tyliszczak and Boguslawski [93], Le Ribault et al. [55] and Bodony and Lele [10] where noise generated from heated and unheated jets where investigated. The LES performed by Wang et al. [96] gives a detailed comparison between experimental and numerical studies for round jets with three different density ratio values.They replicated the experiment conditions of Amielh et al. [2] and Djeridane et al. [31] in their numerical study. For plane jets, only slightly heated jets having density ratios between 0.8 and 0.9 were considered in Jenkins and Goldschmidt [48], Davies et al. [28], Bashir and Uberoi [7], Antonia et al. [4], Browne et al. [14] and Ramaprian and Chandrasekhara [79]. These values do not change the evolution of jet significantly. Foysi et al. [35] also performed numerical studies for plane jets with different density ratios and obtained a good agreement between experiments and numerical study and provided further insight into round-jet/plane jet anomaly [78]. The occurrence of global instability in variable-density flows is also an important phenomenon. Kyle and Sreenivasa [54], Monke-

witz [68], Raynal et al. [80], Hallberg andStrykowski [41], Lesshafft et al. [56] and Nichols et al. [71] reported that above a value of 0.5-0.6, the variable density jets evolve just as the constant density jets.

The density change can also be obtained by heating turbulent jets. These mechanisms are common in nature and need to be extensively studied to predict different combustion situations. Experiments with heated jets have been documented [77, 84]. Mi et al. [64] studied the effect of initial conditions on the scalar field of a heated jet at a Reynolds number of 16000. The jets were issued from two different nozzle types, and experiments were performed for both. Anderson and Bremhorst [3] performed heated turbulent jet experiments and reported various turbulent quantities like mean values, root-mean-squared velocities, and temperature. Self-similarity laws also have been deduced for heated jets from different experiment data for the mean velocity and temperature fields which can be found in Chen and Rodi [24]. Bodony and Lele [10] used LES to predict noise from cold and heated turbulent jets for higher Mach numbers. Similarly, Zhou et al. [108] studied heated turbulent jets at low Reynolds number, investigating the inertia-dominated zone. Smith et al. [87] performed RANS simulation of a heated jet to study the effect of different nozzle shapes on the flow physics. Suto et al. [91] simulated four different Reynolds numbers for a heated jet using LES. Significant disparities were found in the near-field scalar fluctuation intensity for the LES and experimental measurements. Colombo et al. [25] performed LES of a heated jet using FLUENT to measure mean velocity, mean temperature but study of rms temperature fluctuations was missing in this study.

RANS models like the standard K-epsilon, Realizable k-epsilon have several limitations to jet flow modeling with three-dimensionality, compressibility, and high-temperature effects. For different types of jets at higher Reynolds numbers, jets tend to have higher energy in small scales at the nozzle vicinity which becomes challenging for LES with higher mesh resolution and low timestep requirements increasing the computational cost of simulation. Direct Numerical Simulation resolves all turbulent motions down to the Kolmogorov scale

and calculates the whole turbulent spectrum. However, it is severely limited by the computational resources required. So, an alternative method for turbulent jet modeling using deep learning is discussed.

Artificial Neural Networks (ANNs) present an excellent alternative for modeling unsteady flow dynamics. An artificial neural network (ANN) is a computing system designed to simulate how the human brain analyzes and processes information. Processing units make up ANNs, which in turn consist of inputs and outputs. The inputs are what the ANN learns from to produce the desired outcome. To predict the expected output, a number of parameters has to be trained for any ANN. These parameters are known as global hyperparameters, which affect the error function or the loss function. The goal is to tune these parameters in such a way that the loss function can be minimized [101]. Various types of ANNs are available depending upon their architecture, the number of nodes, types of activation function used. For instance, Recurrent neural networks (RNNs) are neural networks that cycle past outputs back to the network as inputs while maintaining hidden states. ANNs have been historically combined with other techniques such as NARMAX to predict highly nonlinear chaotic systems such as the Lorentz system [99] and Sunspot time series [106]. Chandra and Zhang [18] used neural networks to predict chaotic time series data. Their work included training Elman recurrent neural networks on chaotic time series problems. They used the Mackey-Glass, Lorenz, and Sunspot time series to demonstrate the performance of the cooperative neuro-evolutionary methods. They appeared to achieve improvement in terms of accuracy compared to other methods. Diaconescu [30] used a Recurrent Neural Network (RNNs) with many neurons to capture the dynamics of nonlinear dynamic systems such as the Mackey-Glass system. A recurrent predictor neural network (RPNN) consisting of linear nodes was used by Han et al. [42] to model and predict chaotic time series. A backpropagation through time (BPTT) learning algorithm was used to train the neural network. Long Short Term Memory (LSTMs) neural networks were proposed by Vlachas et al. [95] for forecasting high-dimensional chaotic systems. It seemed to outper-

form the Gaussian Processes (GPs) in short-term forecasting for all the systems considered. Recurrent Neural Networks (RNNs) represent powerful machine learning tools capable of solving real-world temporal problems like prediction and robotics. However, training RNNs is a difficult task. Error backpropagation methods have been used to train RNNs with some success [9, 22]. One of the primary limitations of this method, as indicated by Chatzis and Demiris [23] is the training process becomes non-converging due to bifurcations. Slow convergence and high computational costs of RNNs also limit its utility for practical applications. However, a significant limitation of RNNs is the vanishing gradient problem which severely limits their ability to learn long data sequences. Despite these challenges, attempts to extend the potential of ANNs continue, as does the range of phenomena represented by ANNs. ANNs have already been used to simulate turbulent flows, which is relevant to this research. Gamahara and Hattori [36] used Artificial Neural Network (ANN) as a tool for finding a new sub-grid scale model of the sub-grid scale tensor in Large Eddy Simulation. A feedforward neural network was used to establish relation between the flow field and sub-grid scale tensor. The friction factor of an open channel flow was predicted and compared to the value obtained from the empirical formula using a three layer ANN in Yuhong and Wenxin [102] and a reasonable agreement was found. In Babcock et al. [6] a neural network was used to learn a function nearly identical to an analytically derived control law. They demonstrated the ability of a neural controller to maintain a drag-reduced flow in a fully turbulent fluid simulation. ANNs are also used in combustion problems to hasten sub-grid chemistry computations [46, 83]. In a large portion of these works, be that as it may, ANNS were utilized uniquely as a correlative device for advancing model constants.

An alternative to gradient descent methods was thus proposed by Jaeger [47] as the Echo State Network and by Maass et al. [62] as the Liquid State Machine in which only the synaptic connections from the RNN to output neurons were trained by learning. The ideas of Echo State Network and Liquid State Machines were unified into a common research

topic known as the 'Reservoir Computing' (RC) [94]. The idea of ESN can be traced back to Neuroscience. Domine [32] presented an algorithm of the brain, which was the actual precursor of ESN. In the echo state network, the input weights and weights of the RNN (reservoir) are randomly generated, and only the readout layer from the reservoir to the output layer is trained [34]. Several global hyperparameters must be tuned for successfully implementing the Echo State Network. Application of ESN so far include speech recognition [86] , robot control[5] , forecasting financial market[57] and dynamical systems such as the Mackey-Glass system [63]. An important aspect for the Echo State Network to work is the reservoir must have the echo state property. It states that the effect of an earlier state or a previous input should vanish on the future state as time passes [39]. Mathematically, the echo state property is assumed to be maintained if the spectral radius value (the largest eigenvector) ρ(W) of the reservoir weights is less than or equal to a value of 1. However, the echo state property holds for $\rho(W) \geq 1$ for nonzero inputs u(n) so $\rho(W) < 1$ is not necessary condition for the echo state property [61, 97]. Reservoir computing has been primarily used to model chaotic time series dynamical systems. ESNs in the current literature have been found to use three configurations while predicting chaotic behaviors, namely, observer mode (or non-autonomous mode) where model free prediction is achieved with limited state variables [60], the feedback (or autonomous) mode in which during the prediction, the output of a previous timestep is fed as the input in the reservoir[59, 75] and finally custom ensemble methods where ESNs are used in conjunction with knowledge-based models[74]. Pathak et al.[75] used Reservoir Computing to create a model-free estimation from data of Lyapunov exponents of a chaotic process. They used the Lorentz system and the Kuramoto- Sivashinsky (KS) equation to validate their method. Krishnagopal et al. [53] studied the effectiveness of reservoir computing for separation of chaotic signals and concluded that their results were better than the Wiener filter obtained from the same training data. Reservoir computing has also been used for short-term prediction, and attractor reconstruction of a chaotic system from time-series data [59]. Pathak et al.

[74] combined machine learning technique and knowledge of the mechanical processes to build a hybrid forecasting scheme for the prediction of dynamical system states. Several studies have been performed to understand the dynamics of Reservoir computations to enable effective prediction of dynamic systems. Carroll [15, 16, 17] used RC-ESN at the edge of chaos to perform predictions and concluded that it does not necessarily improve the performance. A study in the sensory phase with two parallel reservoirs was conducted by Zhang et al. [105] and concluded that parallel reservoirs are limited in collecting dynamics of a coupled chaotic system of the entire system in the long run. Turbulence has also been studied using Reservoir Computing. The large-scale development of two-dimensional Raleigh-Benard convection was evaluated using Reservoir Computing by Pandey and Schumacher [73]. Rayleigh-Benard convection problem was studied, and temperature fluctuations were predicted using Reservoir Computing by Chang and Lathrop [19]. Kalogirou [51] discuss the use of ANNs in combustion related engineering problems.

The rest of the dissertation is organized as follows: Chapter 2 discusses the successful implication of an ESN to model incompressible round jet behavior. In Chapter 3, a heated jet is modeled and compared to experiments using an ESN. Variable-density jets are studied with an ESN in Chapter 4. Finally, the conclusions of this dissertation are presented in Chapter 5.

1.2 Motivation

The modeling of turbulent flows has a long history, and turbulence is still considered one of the most important yet unsolved engineering problems. Turbulent jet flows are observed in a myriad of engineering technologies such as fuel/oxidizer injectors, thermal management technologies, industrial smokestacks, etc. The essential features of a turbulent jet, such as mixing and noise generation, are closely associated with the development of turbulence generated by shearing flows. ESNs represent an advantage over traditional models in that they do not require solving the unsteady Navier-Stokes equations. ESNs do require a knowledge of an associated flow field time series as input to the so-called reservoir. Once the ESN is trained, future flow field time series may be predicted. Simply put, ESNs provide a model-free estimation of turbulent flow behavior. An extensive literature review has revealed that ESNs have successfully modeled the dynamical behavior of the Lorentz, Rössler, and Mackey Glass systems. The use of ESNs extends beyond academic mathematical research. Such networks are also currently used in the business community for digital asset management and call center data analysis.

The proposed effort will benefit society by providing an alternative to turbulence modeling with the use of an Echo State Network, a field with far-reaching industrial and scientific applications. By creating a computationally efficient framework for accurately predicting turbulent jet flow behavior, the research will lay the groundwork for the future development of turbulence models. Machine learning has already been successfully applied to several disparate fields. The proposed research will continue to expand the use of machine learning and artificial intelligence into fluid dynamics.

The current study will contribute to turbulent jet modeling by using Deep Learning to study turbulent jet flow behavior. A massively parallel ESN architecture will be developed and will be used to create a model-free estimation of turbulent jet behavior. ESN is a data-driven model, which does not need any physical information of the system from which the data is generated.

1.3 Objectives

The project goals will be accomplished by successfully meeting the following objectives. The data for all the jet configurations will be obtained by performing a Large Eddy Simulation in a commercially available CFD software.

- An existing framework of Echo State Networks (ESN) available from an open-source GitHub repository is built upon and modified extensively to model the incompressible round jet behavior.
- An existing framework of Echo State Networks (ESN) available from an open-source GitHub repository is built upon and modified extensively to model the heated jet behavior.
- An existing framework of Echo State Networks (ESN) available from an open-source GitHub repository is built upon and modified extensively to model the variable-density jet behavior.

CHAPTER 2

ON THE USE OF RESERVOIR COMPUTING (ECHO STATE NETWORKS) TO PREDICT THE BEHAVIOR OF INCOMPRESSIBLE TURBULENT JETS

2.1 Abstract

The effectiveness of using an Echo State Network (ESN) to predict the characteristics of turbulent flow fields is explored. ESNs are a particular class of recurrent neural networks that have previously been shown effective for modeling highly transient behavior. In this study, the model problem is a turbulent free jet issuing from a circular tube into a quiescent medium. The results presented represent the first time an ESN has been used to model turbulent free jets. Reynolds numbers of 3600, 10^4, and 10^5 are compared with previously published turbulent flow results. ESN training is achieved using a validated LES dataset obtained from commercially available CFD software. A separate LES dataset is used to evaluate how well the ESN predicted flow field behavior. A hyperparameter search is undertaken to enhance the ESN's ability to model the turbulent flow field under consideration. The ESN model proved capable of reproducing instantaneous vortical structures and centerline velocity behavior relative to LES model data and previously published experimental data. The ESN model results accurately predict the frequency corresponding to the shear layer mode, as calculated by inviscid instability theory. In addition, the ESN model accurately predicts that the jet-preferred mode's dependency upon the Reynolds number and the initial momentum thickness. Modal analysis of the ESN results correctly indicates that near the shear layer, mode 0 is dominant, while past the potential core mode 2 is dominant. Based on the results of this study, it is clear that an ESN has the potential to model turbulent flow fields effectively.

2.2 Introduction

As turbulent flows are ubiquitous in both nature and engineering applications, the importance of predicting the behavior of such flows cannot be overstated. Turbulence impacts a myriad of phenomena known to influence ecological as well as biological systems. From a technological perspective, predicting the behavior of turbulent flows is often critical to the design and sizing of components in complex engineering systems. Unfortunately, turbulent flow behavior is, in itself, highly complex. Turbulent flows are inherently three-dimensional, unsteady, and chaotic. The vortical structure within a turbulent flow field produces an energy cascade from the largest integral length scales through the intermediate Taylor microscales to the Kolmogorov microscales, below which viscosity transforms kinetic energy to thermal energy. This turbulent energy cascade results in a flow field with a wide range of relevant length and time scales, all of which must be accurately modeled to capture the associated dynamical behavior. As such, the computational expense of simulating turbulent flows often limits the practical prediction of flow characteristics. Given the importance of turbulent flows, it is not surprising that a large body of research has been devoted to the modeling and simulation of turbulence.

Past efforts to model and simulate turbulent flows have primarily involved the use of either the Reynolds-Averaged Navier-Stokes (RANS) equations, the Large Eddy Simulation (LES) technique, or Direct Numerical Simulation (DNS). The RANS equations are obtained by representing the instantaneous velocity as the sum of time-averaged and fluctuating velocity components. The resulting formulation is not closed and requires modeling of the so-called Reynolds stresses. Numerous Reynolds stress models have been developed over the years. The validity of these models is often closely tied to the physical configuration of the flow field, thus limiting the use of a given model. In addition, certain Reynolds stress models require the solution of additional differential equations, thus increasing the computational expense of modeling turbulence in this manner. Yusuf et al. [103] presented an overview of turbulence modeling using the RANS equations in the context of indus-

trial flows. Xiao and Cinnella [100] reviewed parametric and structural uncertainties in turbulence models. Also presented was a review of the uncertainties encountered with approaches such as LES. In LES, the scale to which the larger scale vortical structures of a flow are simulated, not modeled, is determined by the application of a low-pass filter to the Navier-Stokes equations. This approach also produces a closure problem, which is addressed through the use of a Sub-Grid Scale (SGS) model to account for phenomena not explicitly captured by the resolution of the computational grid. While the LES approach does allow for the intentional control of what is simulated versus modeled, higher fidelity simulations increase the computational expense of this approach, and for certain classes of turbulent flows, there are still inaccuracies in the available SGS models. Zhiyin [107] discuss the history of using LES for solving complex turbulent flows. Ideally, one would prefer to resolve all scales of turbulent motion down to the Kolmogorov scale and eliminate the need for a turbulence model. This approach is that taken by DNS. In Moin and Mahesh [67], a multifaceted discussion of the challenges associated with DNS is provided. To date, DNS has proved invaluable for accurately simulating the physics of certain idealized flow configurations and for complementing experimental efforts to understand turbulent flows. Unfortunately, grid resolutions required to capture the entire turbulent spectrum make DNS the most computationally expensive technique for predicting turbulence flow behavior. At present, this prohibits the use of DNS for anything other than the simplest flow geometries.

Turbulent jets represent a classical problem in turbulent flow modeling. The development of turbulence caused by shearing flows is strongly connected with the basic properties of a turbulent jet, such as mixing and noise generation. Previous research has used a variety of turbulence models in conjunction with the RANS equations and subgrid-scale turbulence models linked with the LES approach to simulate turbulent jets and study the impact of jet inflow conditions. Bogey and Bailly [11] used LES to study jet inflow condition effects at a Reynolds number of 4×10^5. Kim and Choi [52] used LES to investigate the

impact of jet entrance conditions on jet flow characteristics. They discovered that the jet behavior are strongly influenced by the momentum thickness of the jet and the Reynolds number. Jets tend to have more energy in small scales around the nozzle vicinity at higher Reynolds numbers, requiring fine grid resolution and increasing the computation cost.

A promising alternative to traditional turbulence modeling techniques involves the use of Artificial Neural Networks (ANNs). ANNs are modeling algorithms that may be thought of as computational analogues to biological neural networks. In the most basic sense, an ANN is comprised of a network of artificial neurons, i.e., nodes. Each node receives a weighted sum of input from other nodes and/or from the input to the network and maps this to the node's output using a predefined activation function. With the appropriate weighting of the various inputs to the nodes, ANNs can predict the behavior of highly nonlinear, multidimensional functions and phenomena. In addition to the structure of the nodal network itself, a key consideration for ANN implementation is how the respective weighting functions are updated via a learning algorithm. Multiple ANN architectures have been developed, and these differ in terms of structure, the number of node layers (hidden layers), node density, data flow, learning algorithms, and activation function. For example, the widely used and effective Recurrent Neural Network (RNN) architecture loops data from the output layer back into the neural network in a manner that allows for the prediction of sequential behavior. Both Chandra and Zhang [18] and Diaconescu [30] used RNNs to predict the behavior of chaotic times series. RNNs are not without their challenges. The process of training the RNN, i.e., adjusting the nodal weighting functions to minimize modeling error, becomes increasingly difficult as the number of nodes increases. Bishop [9] and Chatzis and Demiris [22] used the error backpropagation approach, with some success, to train RNNs. One of the primary limitations of this approach, as indicated by Chatzis and Demiris [22], is that the training process becomes non-convergent when bifurcations exist. The so-called vanishing and exploding gradient problems may also drastically slow down the RNN training process. Despite these issues, efforts continue to expand the capabilities

of ANNs, and the breadth of phenomena being modeled by ANNs continues to increase. With particular interest to this study, ANNs have previously been used to model turbulent flows. A friction factor model for turbulent open channel flow was developed by Yuhong and Wenxin [102] using a 3-layer ANN. Gamahara and Hattori [36] utilized an ANN to develop a Sub-Grid Scale model for use in LES. Babcock et al. [6] developed a controller for reducing drag in 3-dimensional turbulent flows using ANNs. Mohan et al. [66] used yet other more advanced ANN architectures, physics-informed deep learning models, to predict the behavior of 3-dimensional isotropic turbulent flows.

Echo State Networks (ESN) represent an ANN architecture that alleviates specific issues with RNNs and has been previously used to model highly transient behavior. ESNs were first proposed by Jaeger [47], and together with the Liquid State Machine architecture proposed by Maass et al. [62], came to be known as the Reservoir Computing (RC). In an ESN, the input weights and RNN (reservoir) weights are generated randomly, and only the readout layer from the reservoir to the output layer is trained. This enables faster training, compared to traditional RNNs, thus lowering the computational expense of training - one of the most significant advantages of ESNs [47]. In order for the Echo State Network to function properly, the reservoir must have the so-called echo state property. The echo state property asserts that as time passes, the influence of a prior state or previous input should fade away [39]. Tanaka et al. [92] provided a comprehensive assessment of recent improvements in reservoir computing methods based on the type of reservoir employed. ESNs have largely been applied to the simulation of chaotic temporal dynamical systems. Pathak et al. [75] utilized Reservoir Computing to construct a model free estimation, using Lyapunov exponent data, for a chaotic process. The authors validated their technique using two examples: the Lorentz system and the Kuramoto-Sivashinsky (KS) equation. Krishnagopal et al. [53] investigated the usefulness of reservoir computing for chaotic signal separation and found that the results were superior to the Wiener filter. Short-term prediction and attractor reconstruction of a chaotic system from time series data have been

accomplished using reservoir computing [59]. Reservoir Computing has also been used to model turbulent flow analogues. Pandey and Schumacher [73] used Reservoir Computing to evaluate the large scale evolution of a two dimensional Raleigh-Benard convection. Reservoir Computing was used to predict temperature fluctuations in a Rayleigh-Benard convection problem by Chang and Lathrop [19]. ANNs and ESNs represent an alternative to the classical approaches to modeling turbulence as ESNs do not require solving the unsteady Navier-Stokes equations. The past success of using the ANN approach motivated the present study.

Incompressible turbulent jet flow has been modeled using an Echo State Network (ESN). This is the first time an ESN has been used to model a turbulent free jet. To assess the effectiveness of the ESN, the ESN model data was compared to a separate LES data set and to previously published turbulent jet flow results. The mathematical formulation used to obtain the LES training and testing data is presented in §3.3, as is a summary of the computational solution approach and the validation of the LES results. A description of the ESN model is presented in §3.4. The ESN training and testing procedures are also presented in this section. The results of the ESN training, including the results of the hyperparameter search, are given in §3.5. The ability of the ESN to capture the salient features of a turbulent free jet is also explored in §3.5, with particular emphasis placed on reproducing the vortical structure, the centerline flow behavior, and the modal properties of the turbulent jet. The conclusions drawn from the results of this study are outlined in §3.6.

2.3 Large Eddy Simulation

The mathematical and computational formulation used to model the turbulent jet, using LES, is outline below.

2.3.1 Mathematical Formulation: Turbulent Jet

Consider the flow of a fluid as it exits a circular pipe into a quiescent medium. Filtering the time-dependent Navier-Stokes equations in either Fourier (wave-number) space or con-

figuration (physical) space yields the governing equations for LES. The filtered governing equations of an incompressible viscous flow for LES are

$$\frac{\partial \widetilde{u}_i}{\partial x_i} = 0 \tag{2.1}$$

$$\frac{\partial \widetilde{u}_i}{\partial t} + \frac{\partial \widetilde{u}_i \widetilde{u}_j}{\partial x_j} = \frac{\partial}{\partial x_j}\left(\sigma_{ij}\right) - \frac{\partial \widetilde{p}}{\partial x_i} - \frac{\partial \tau_{ij}}{\partial x_j} \tag{2.2}$$

where $\widetilde{u}_i$ denotes filtered velocity components, x_i are the spatial coordinates, $\widetilde{p}$ is the filtered pressure field, σ_{ij} denotes the stress tensor owing to molecular viscosity, i.e., μ, defined as

$$\sigma_{ij} = \left[\mu\left(\frac{\partial \widetilde{u}_i}{\partial x_j} + \frac{\partial \widetilde{u}_j}{\partial x_i}\right)\right] - \frac{2}{3}\mu\frac{\partial \widetilde{u}_l}{\partial x_l}\delta_{ij} \tag{2.3}$$

and

$$\tau_{ij} = \widetilde{u_i u_j} - \widetilde{u}_i \widetilde{u}_j \tag{2.4}$$

is the sub-grid stress scale. The sub-grid scale stresses must be modeled, which in this study is done using the widely used Dynamic Smagorinsky-Lily model proposed by Germano et al. [38].

The problem domain is shown in figure 2.1. Far field boundary conditions were applied at the side boundary $r = L_r$ $(\partial(ru_r)/\partial r = 0, \omega_x = \omega_\phi = 0)$ where ω denotes vorticity, the domain boundary downstream of the jet outlet $x = L_x - L_j$ $(\partial(u_x)/\partial x = 0)$, and the domain boundary upstream of the jet outlet $x = -L_j$ $(\partial(u_x)/\partial x = 0)$. Upstream of the jet exit, along the wall $(L_j \leq x < 0, r = D/2)$, a Blasius profile was used following Kim and Choi [52]. At the jet exit $(x = 0, 0 \leq r \leq D/2)$, i.e., the core area, a constant velocity, $u_x = U_j$, boundary condition was applied. Superimposed on this value was a random fluctuation of 0.01. This value was chosen for the simulations in this study to align with the LES results of Kim and Choi [52]. For each Reynolds number, the domain dimensions were selected to

be equivalent to Kim and Choi [52]. In addition, Reynolds numbers of 3600, 10^4 and 10^5 were considered and a ratio of the diameter to the momentum thickness of $D/\theta = 50$, for the Blasius profile, was also used to align with the work of Kim and Choi [52].

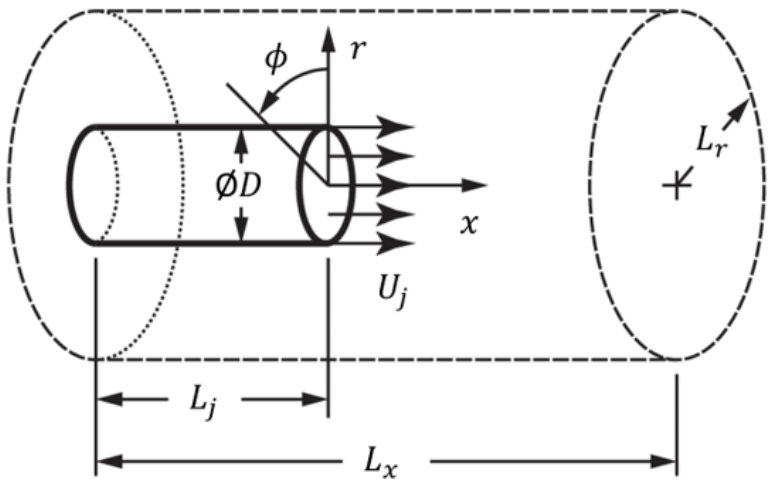

Figure 2.1: Computational domain used for LES Simulation.

2.3.2 LES: Computational Implementation

For each Reynolds number, prior to the solving the problem using LES, an initial RANS model was solved using the above boundary conditions to check the convergence of the solution. The mean velocity profile from the RANS results was then used as an initial conditions for LES.

The Courant number was set in such a way that it never exceeded 0.1. The computational mesh was composed of hexahedral cells only. In the axial and radial directions, geometrically dispersed non-uniform spacings were employed, with minimum values at $x = 0$ and $r = 0.5D$ corresponding to $\Delta x/D = 0.01$ and $\Delta r/D = 0.00781$. To capture the velocity gradients in the shear layer, the minimum cell spacing in the radial direction was calculated using a value of $r^+ = 2$ (enhanced wall treatment was used), estimated using Blasius law for smooth pipes, i.e., $C_f = 0.0791Re^{0.25}$, and having 16 cells in the range of $0.4 < r/D < 0.6$. The mesh's full-scale resolution in the z-plane, as well as the jet inlet,

are shown in figure 2.2.

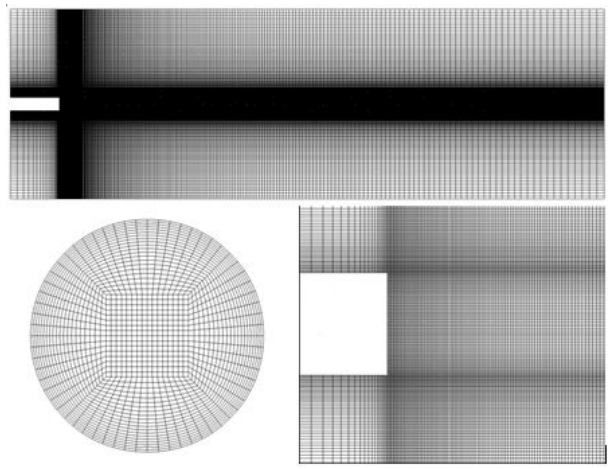

Figure 2.2: Schematic of a typical mesh used for the LES simulation.

The governing equation were integrated in time using the Bounded Second-Order Implicit scheme with a fixed time step of $\Delta t = 0.00633D/U_j$, ensuring a CFL 0.1. Pressure-velocity coupling was achieved using the Fractional Step method. The Least Squares method was used for computing gradients and central differencing was used for pressure and convective term interpolation.

2.3.3 LES: Verification and Validation

Three different grid spacings in the axial direction were explored. In the axial direction, grid spacings of $\Delta x_{min}/D = 0.005, 0.01$ and 0.02 were used. Between $\Delta x_{min}/D = 0.005$ and $\Delta x_{min}/D = 0.01$ the maximum difference in the mean axial velocity along the centerline was on the order of 0.02. Based on this, a minimum grid spacing of $\Delta x_{min}/D = 0.01$ was chosen for all the the LES cases during the course of the study. Using this grid resolution resulted in a computational mesh of 3, 6, and 8 million cells for $Re_D = 3600$, 10^4, and 10^5, respectively. As with many aspects of the LES cases, these values are comparable to those used in Kim and Choi [52]. As for the validation of the LES results, it is shown in §3.5 that the LES data obtained in this study compared favorably to previously published computational and experimental data.

2.4 Echo State Network

An Echo State Network (ESN) consists of an input vector $u(t)$ with K units, that feed into a dynamic reservoir with N units. The reservoir is coupled to an output layer $y(t)$ with N_y units as described by Pathak et al. [74]. The reservoir receives input at a discrete time t, which is then coupled with the reservoir state to produce its output at $t + \delta t$.
An ESN is fundamentally an RNN with fixed, randomly generated weights in the hidden (reservoir) layer [61]. The update equations for an ESN are:

$$\widetilde{x}(n) = \tanh(W^{in}[1; u(n)] + Wx(n-1)) \tag{2.5}$$

$$x(n) = (1-\alpha)x(n-1) + \alpha\widetilde{x}(n) \tag{2.6}$$

where $x(n-1)$ is the reservoir node activation at a previous time step, $x(n)$ represents reservoir node activation at the current time step, and $\widetilde{x}(n)$ represents the intermediate update at each time step n. The sigmoid function tanh(), used in this study, is one of the most popular choices for an activation function. The leaking rate is $\alpha \in (0,1]$, the symbol [;] represents a vertical vector (or matrix) concatenation. The input weight matrix and recurrent weight matrix are W^{in} and W, respectively [61]. The output weight matrix is constructed using Ridge regression after the reservoir has been trained. The linear readout layer's definition is as follows:

$$y(n) = W^{out}[1; u(n); x(n)] \tag{2.7}$$

The original ESN technique, as outlined by Jaeger [47], is:

- Create a random reservoir using the input weight matrix W^{in}, the recurrent weight matrix W, and the leaking rate α.
- Run the network with the training input $u(n)$ and gather reservoir activation units $x(n)$.

- Calculate the network output using the linear readout. Calculate W^{out} output weights by minimizing the difference between the network output and the target output.
- Compute output using the trained network with the new input data.

2.4.1 ESN Training

For a given Reynolds number, the resulting LES data set was divided into two distinct sets, one set for training and a different set for testing. The so-called LES training data set was used as the input for the ESN reservoir, which then produced the initial ESN output. The initial ESN output was then compared to the LES training data set and the error associated with the ESN output was calculated using

$$E(y, y^{t\arg et}) = \frac{1}{N_y}\sum_{i=1}^{N_y}\sqrt{\frac{1}{T}\sum_{n=1}^{T}\left(y_i(n) - {y_i}^{t\arg et}(n)\right)^2} \tag{2.8}$$

where E is the associated error, N_y the number of output dimensions, T is effectively the number of data points of the training set, y_i is the initial ESN output, and y_i^{target} is the corresponding LES training data set value. The output weights were then adjusted by minimizing the least square error between the initial ESN output and the target values [61, 85]. As discussed in §3.5, there are several hyperparameters that may be tuned to enhance the training process and increase the effectiveness of the ESN model.

2.4.2 ESN Testing

As previously mentioned, for a given Reynolds number, the resulting LES data set was divided into two distinct sets, one set for training and a different set for testing. Once the ESN output layer training is complete, the ESN model is now capable of autonomously predicting the future flow behavior of the turbulent jet under consideration. The so-called LES testing data set was used to compare the effectiveness of the ESN model predictions. At this point, it is important to note that the Echo State Property of the ESN reservoir will not allow longer term predictions of the turbulent jet behavior. This is because over time the driving signal to the reservoir will decrease in magnitude. Since the seminal work

of Lorenz [58], it has been known that longer term prediction of chaotic behavior is not possible. Since turbulent flows are inherently chaotic, it is therefore not possible to make longer term flow predictions and thus the Echo State Property does not necessarily diminish the effectiveness of the ESN approach.

2.4.3 ESN Parallel implementation

Another limitation of the ESN approach is a limitation on the reservoir size. As the number of neurons in the reservoir increases, the computational expense of tuning the hyperparameters increases thus increasing the time needed for creating a functional model that accurately predicts the flow field behavior. This was not a problem for majority of the predictions made during the course of this study. However, when trying to predict the turbulent vorticity field, i.e., the Q-criterion, the number of neurons became prohibitive. To overcome this problem, a parallelized version of the ESN model was developed.

The parallel implementation of the ESN model was accomplished using Open MPI in Python. The flow field was decomposed into several spatial domains. Each spatial domain is predicted by a unique ESN reservoir. Continuity is achieved between two adjacent spatial domains using the concept of the locality parameter. Each reservoir evolves in parallel during training and produces a unique set of output weights. This approach was successfully used by Pathak et al. [74] to predict the dynamics of the Kuramato-Shivansky equation.

2.5 Results and Discussion

The LES training and testing data sets were calculated using commercially available CFD software. The LES data corresponding to a total simulation time of 2.5 seconds. The LES data from $0.0s \leq t \leq 0.1s$ was discarded to remove any initial transient behavior. The LES data from $0.1s < t \leq 1.7s$ was used for the ESN model training while the LES data from $1.7s < t \leq 2.5s$ was used for the ESN model testing.

Data from twenty-five, uniformly distributed locations along the jet centerline were collected to characterize the jet's behavior. Axial data along the shear layer at $0.5 \leq x/D \leq$

2 and $r/D = 0.5$ were also recorded to calculate shear layer mode frequencies. Statistical values were observed by averaging the outputs from the ESN over time for each of the Reynolds numbers considered. However, for a Reynolds number of 3600 only, data from all grid points were recorded so as to allow for the reconstruction of the entire turbulent flow field and calculation of the associated vorticity field.

2.5.1 ESN Hyperparameters

As with all ESN models, several hyperparameters must be specified. For this study, these included the leak rate, α (the parameter controlling the speed with which the neurons respond to the new input), the reservoir size, N (size of the sparely connected hidden reservoir layer), the regularization coefficient, β (used to control the regression coefficients when performing Ridge regression), the reservoir sparsity parameter, χ (the probability of non-zero connections in the reservoir matrix), and the spectral radius, ρ (the largest eigenvalue for the reservoir matrix). For the parallel implementation of the ESN model, the impact of variations in the number of spatial subdomains used to represent the overall domain and in the locality parameter were also examined. While no formal optimization was conducted, a systematic search was undertaken to determine the value of each of the aforementioned hyperparameters so as to enhance the performance of the ESN model. It was found that some of the hyperparameters varied slightly for different Reynolds numbers. The specific tuned hyperparameters used in this study are given in Table 2.1.

Table 2.1: ESN tuned hyperparameters.

Hyperparameters	Re_D=3600	Re_D= 10^4	Re_D= 10^5
Leak rate, α	0.1	0.1	0.08
Reservoir size, N	1000	800	500
Regularization coefficient, β	10^{-07}	10^{-07}	10^{-07}
Reservoir sparsity parameter, χ	0.1	0.1	0.05
Spectral radius, ρ	1.25	1.25	1.25
Number of groups	150	-	-
Locality parameter	2000	-	-

2.5.2 ESN Training Results

For a Reynolds number of 3600, the local difference between the LES training data set and the ESN model data, i.e., the local error, for different locations along the jet centerline is shown in figure 2.3. Note that to better illustrate the variation in the local error, the vertical scale for $x/D = 6$ is different than for the other axial location plots. As can be seen from the figure, once the ESN model has been trained, the local error generally varies between ± 0.5 with the fluctuations in the local error decreasing as one progresses downstream of the jet.

2.5.3 Jet Vortical Structure

For a Reynolds number of 3600, an instantaneous vorticity field, represented as iso-surfaces of the Q-criterion, is shown in figure 2.4. Recall that the Q-criterion is a parameter used to identify vortices and represents regions where the magnitude of the vorticity is greater than the rate of strain. The ESN model results were compared to a Q-criterion plot, published by Kim and Choi [52], and to a Q-criterion plot generated from the LES testing data (generated a part of this study), for a turbulent jet at the same Reynolds number. While the plot by Kim and Choi [52] is not shown here, the ESN model produced results that qualitatively compared well with the results from Kim and Choi [52]. The ESN model also qualitatively compared well with the LES testing data set. The ESN model was able to capture the vortex rings created by the Kelvin-Helmholtz instability at the jet exit. In addition, the shear layer was observed to become unstable at the jet exit, resulting in the formation of vortex rings. As one progresses downstream of the jet exit, the ESN model reproduced the large-scale vortical structures that form due to vortex coupling.

2.5.4 Jet Centerline Velocity

The jet centerline velocity, as predicted by the ESN model, is shown in figure 2.5 and is compared to the current LES testing data set and the data set from Kim and Choi [52]. Figure 2.5 shows that the ESN model is capable of capturing the behavior of the jet centerline velocity. The jet centerline velocity decreases fastest at higher Reynolds numbers.

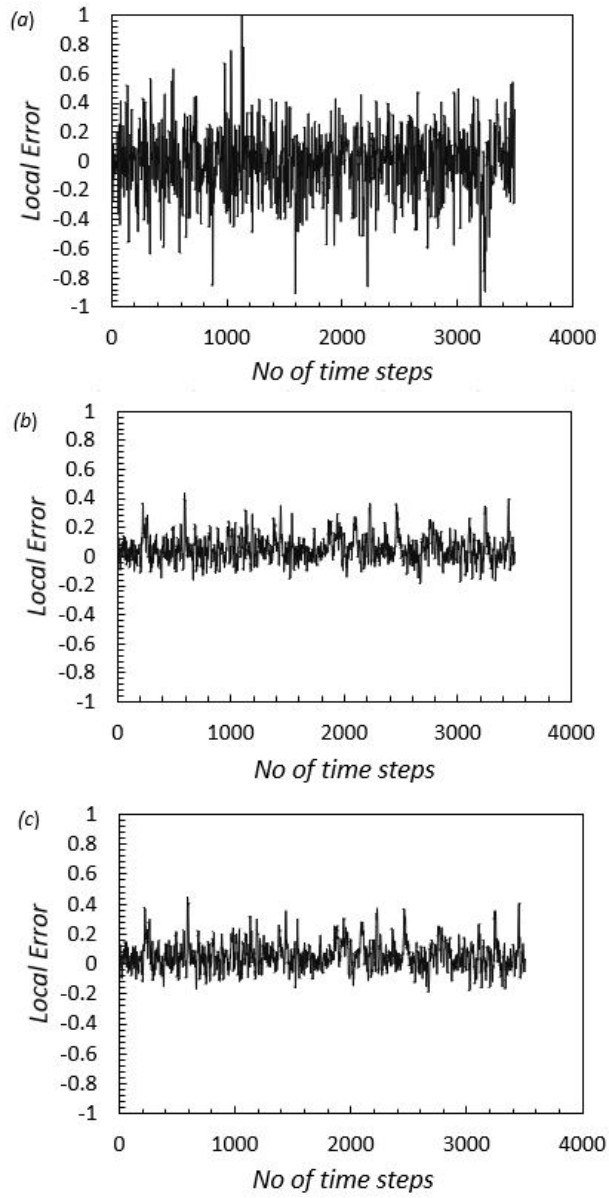

Figure 2.3: Local error plot using an Echo State Network at different locations along the centerline of the jet for Re_D=3600 and D/θ=50, a) x/D=6 (b) x/D=8 and (c) x/D=10.

This is because large-scale turbulent structures form closer to the jet exit at higher Reynolds numbers, reducing the level of jet mixing [104].

Figure 2.6 shows the fluctuations in rms velocity, along the jet centerline, for the three Reynolds numbers considered in this study. The ESN model results are in good agreement with the result from Kim and Choi [52]. A peak value of the rms axial velocity fluctuations was found to occur closest to the jet exit for the highest Reynolds number consid-

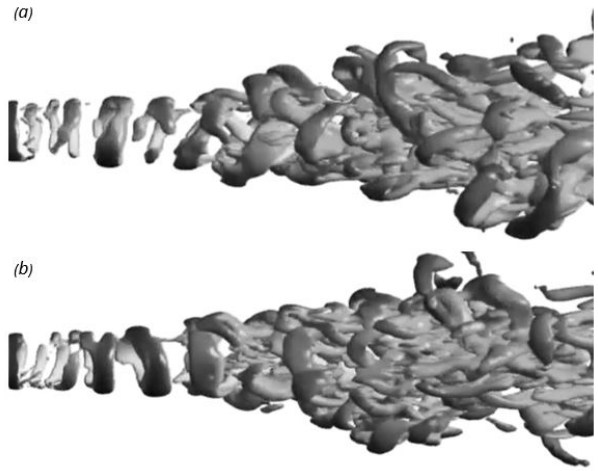

Figure 2.4: Instantaneous vortical structures at Re_D=3600 and D/θ= 50 .a) Large Eddy Simulation (b) Echo State Network Prediction. Shown here are the iso-surfaces of Q criterion at a Q value of 50000.

ered, i.e., $Re_D = 10^5$. The growth in the turbulent intensity, defined as the magnitude of the rms velocity fluctuations, is linked to the formation of large scale turbulent structures.

2.5.5 Instability modes

There exists two instability modes in a turbulent jet; the shear layer mode relating to high frequency oscillations and jet-preferred mode relating to low frequency oscillations. The shear layer mode has a dominant frequency at $St_\theta = 0.017$ [65] or $St_\theta = 0.012$ [104]. For the shear layer mode, the Strouhal number is defined as $St_\theta = f\theta/U_j$ where f is the peak frequency of the energy spectrum for the axial velocity fluctuations, θ is the initial momentum thickness, and U_j is the velocity at the jet exit.

Figure 2.7 depicts the prominent frequencies associated with the shear layer mode. The shear layer frequencies (at $r/D = 0.5$) were calculated from the energy spectra of the axial velocity fluctuations at various axial locations ($0.5 \leq x/D \leq 2$). The energy spectra were obtained after performing an FFT of the axial velocity fluctuations. The peak frequency in the energy spectrum is the dominant frequency along the shear layer ($r/D = 0.5$). According to inviscid theory, the shear layer mode will reach a value of 0.017 when scaled by the initial momentum thickness. The shear layer mode, as predicted by the ESN model was

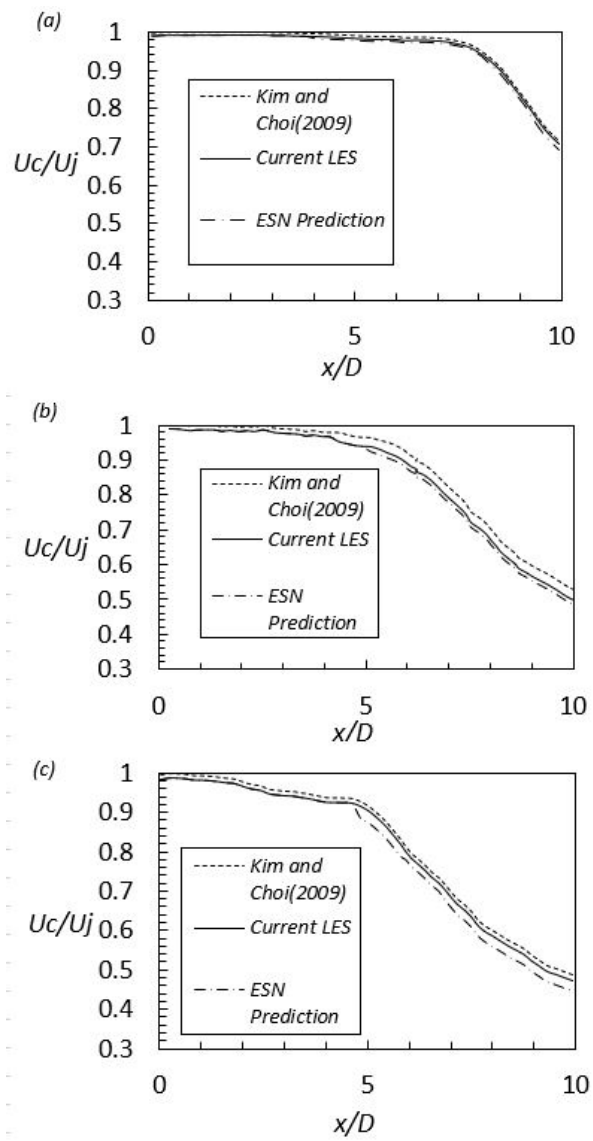

Figure 2.5: Mean axial velocity along the centerline, D/θ=50, $a)Re_D$=3600 $(b)Re_D$=10^4 $(c)Re_D$=10^5.

0.016, i.e., closely reproducing what was expected from inviscid theory. For the shear layer mode, it is traditional to scale the Strouhal number using the jet momentum thickness. If the jet exit diameter is used instead, the ESN model predicted values that were similar to those produced by the ESN testing data (from LES) and by Kim and Choi [52].

According to Gutmark and Ho [40], Ho and Huerre [44] and Kim and Choi [52], the jet-preferred mode frequency ranges from $0.3 \leq St_D \leq 0.6$. For the jet-preferred mode, the Strouhal number is based on the jet diameter, D, and is given as $St_D = fD/U_j$. Figure 2.8

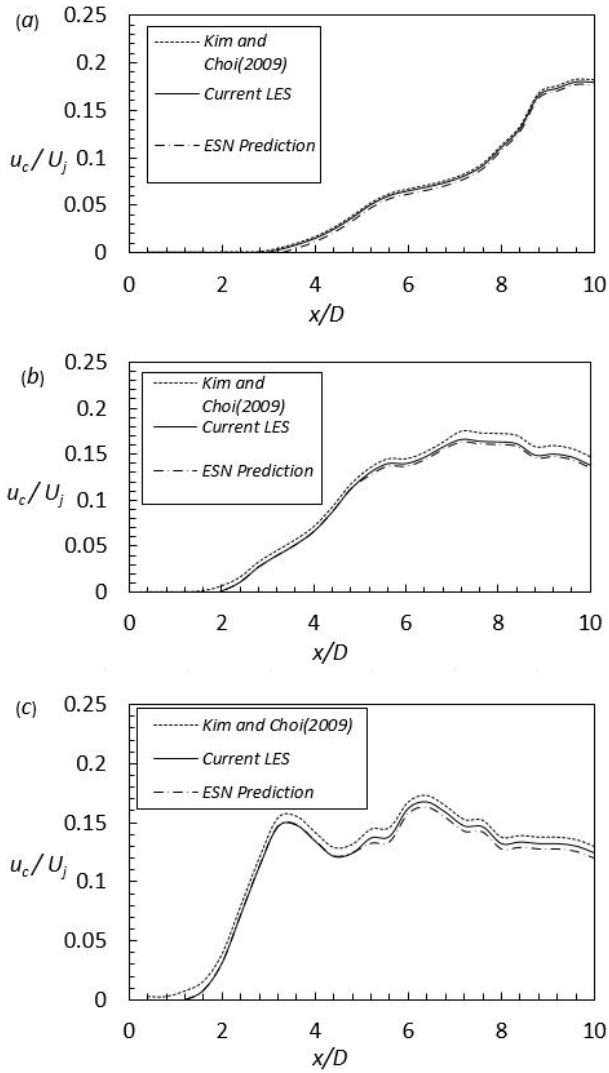

Figure 2.6: rms axial velocity fluctuations along the centerline, D/θ=50, $a)Re_D$=3600 $(b)Re_D$=10^4 $(c)Re_D$=10^5.

shows the primary frequencies associated with the jet-preferred mode. The jet-preferred mode is the dominant frequency obtained at the jet centerline from the energy spectra at $x/D = 4$. The ESN model predicted a range of jet-preferred mode frequencies $0.3 \leq St_D \leq 0.6$, which is consistent with that previously published.

The jet-preferred mode predicted by the ESN model demonstrated increasing agreement with the values calculated by Crighton and Gaster [27] and Petersen and Samet [76] as the Reynolds number increases. Note that for these Strouhal numbers the frequency of the jet preferred mode was scaled by θ_s, the local momentum thickness, and U_c, the local jet

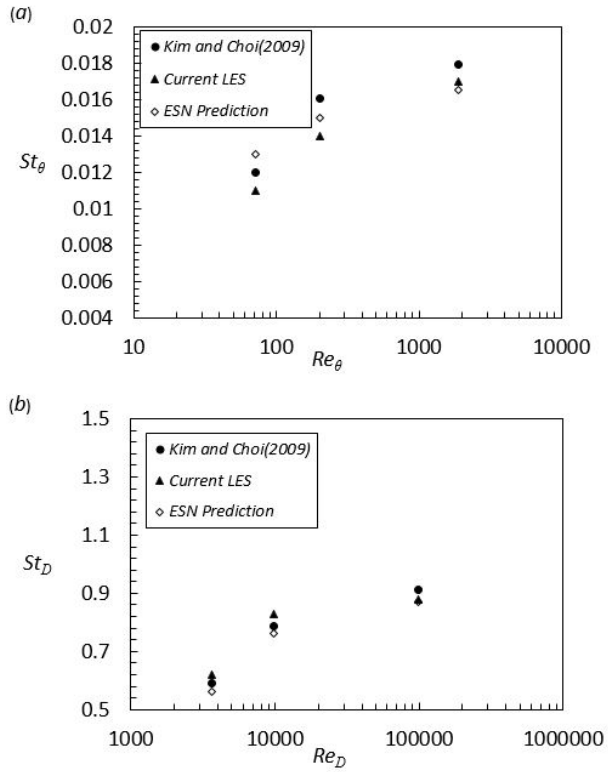

Figure 2.7: Shear layer mode at the shear layer (r/D=0.5), D/θ=50, a) St_θ (b) St_D.

centerline velocity.

2.5.6 Jet Modal Analysis

The vortical structures associated with the turbulent jet were decomposed into the various Fourier components with radial wave numbers of $m = 0$, 1, and 2 corresponding to the axisymmetric, helical, and double-helix modes, respectively. The radial modes in were all found to be unstable at the jet exit, with mode 0 growing the fastest. Mode 1 became unstable beyond the potential core (at approximately $x/D = 4$) and this observed behavior is consistent with the results presented by Batchelor and Gill [8].

Figures 2.9 through 2.11 show the growth of the integrated energy associated with the axial velocity fluctuations for $0 \leq r \leq 2D$ at each radial mode. The Fourier components of axial velocity fluctuations were determined at each time step and axial locations were multiplied with their respective conjugate. The integrated energy values were then obtained by averaging over time. Approaching the jet exit, the ESN model was able to capture that

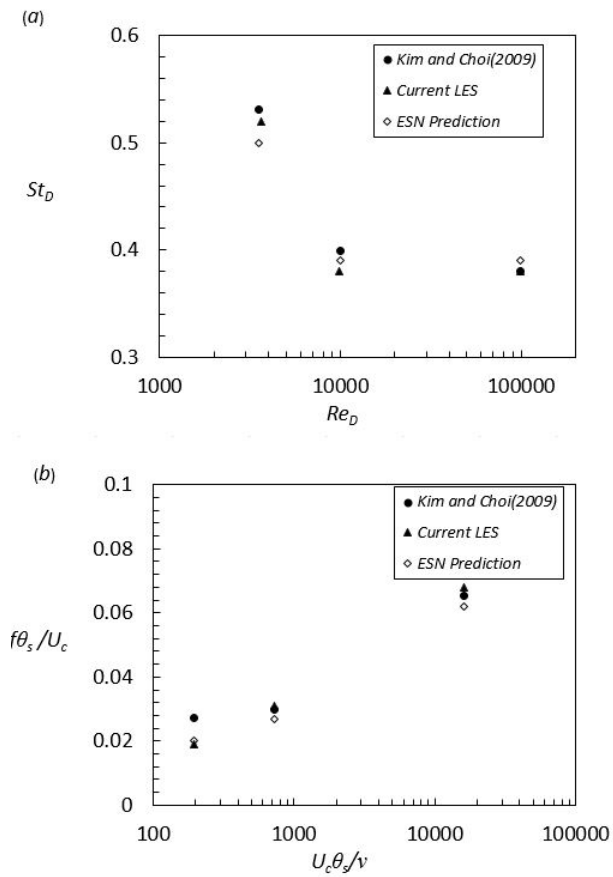

Figure 2.8: Jet Preferred mode , D/θ=50, $a)$ St_D (b) $f\theta_s/U_c$ at x/D=4.

mode 0 was greater in magnitude than the other radial modes. It was also shown that as the Reynolds number increased, mode 0 grew the slowest. Mode 2 became dominant downstream of the jet exit, which is in agreement with the results of Colonius and Freund [26], Jung et al. [50], and Kim and Choi [52]. Kim and Choi [52] observed that the integrated energy of modes 1 and 3 becomes comparable to mode 2 as the Reynolds number increased. This behavior was also captured by the ESN model.

The evolution of radial modes in the shear layer, for $x/D = 4$ and $x/D = 8$ with $0 \leq r/D \leq 2$, was further studied by computing the integrated energy at various axial locations. As seen in figure 2.12, mode 0 increases faster than other shear layer modes towards the jet exit ($x/D = 4$). As one moves downstream toward $x/D = 8$, mode 1 and 2 became the dominant modes along radial direction. This behavior is shown in figure 2.13. In addition, the ESN model predicted that mode 0 would be non-negligible, along the centerline,

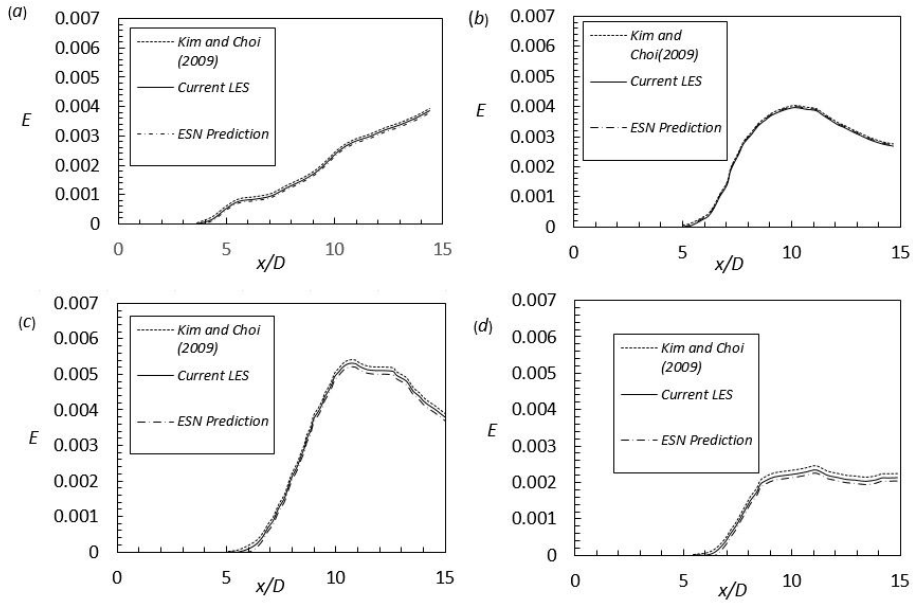

Figure 2.9: Growth of the integrated energy of axial velocity fluctuations Re_D=3600 , D/θ=50,(a) mode 0 (b) mode 1 (c) mode 2 (d) mode 3.

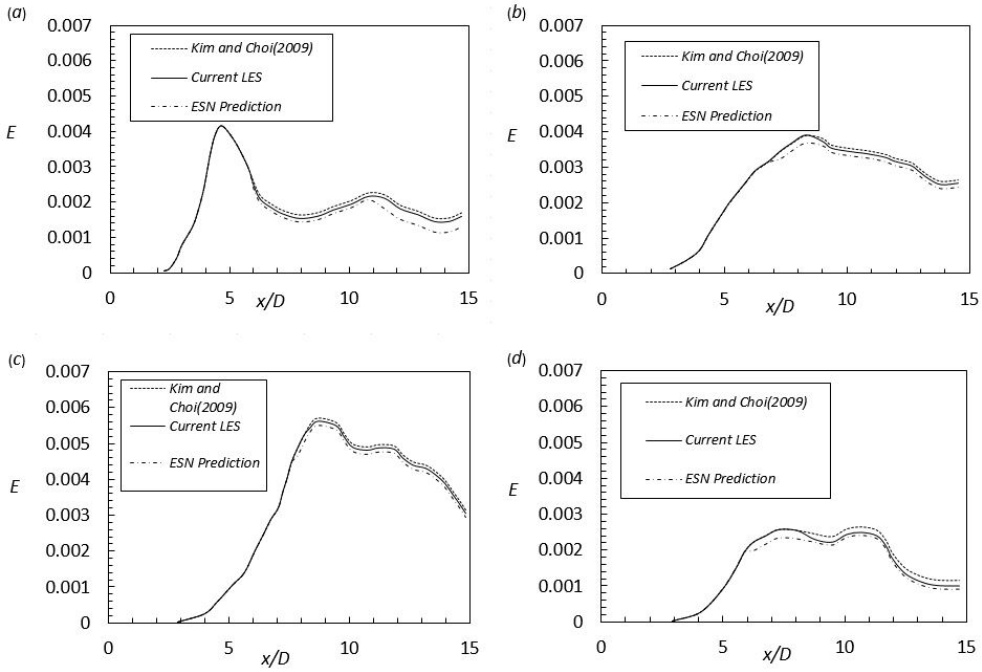

Figure 2.10: Growth of the integrated energy of axial velocity fluctuations Re_D=10^4 , D/θ=50,(a) mode 0 (b) mode 1 (c) mode 2 (d) mode 3.

even at the farthest downstream location. The ESN model predictions, with respect to the evolution of the radial modes in the shear layer, are consistent with the results of Kim and Choi [52].

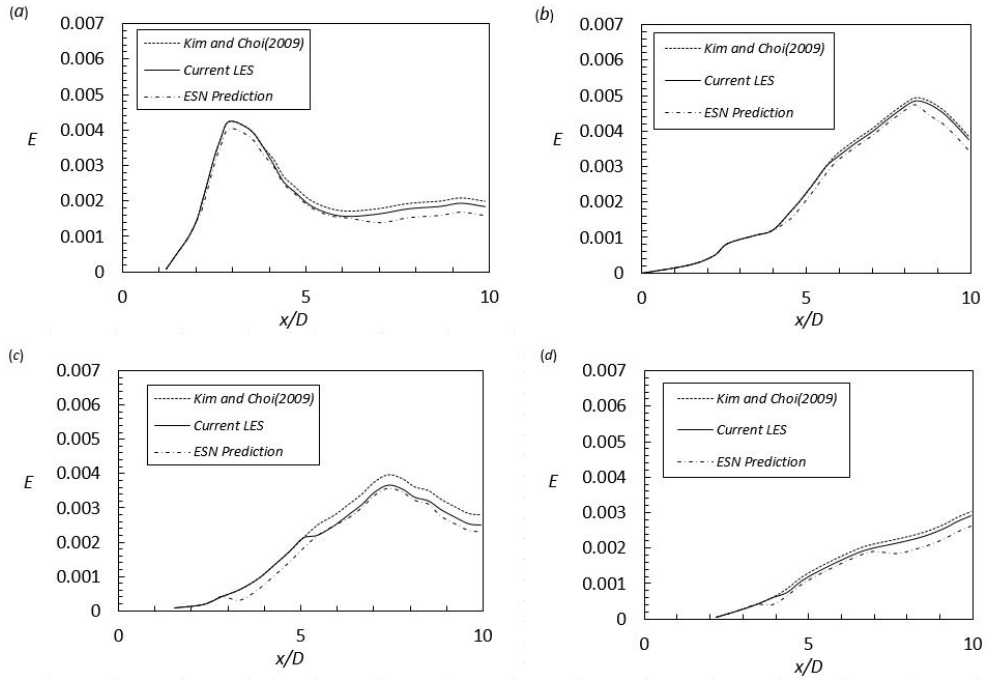

Figure 2.11: Growth of the integrated energy of axial velocity fluctuations Re_D=10^5 , D/θ=50,(a) mode 0 (b) mode 1 (c) mode 2 (d) mode 3.

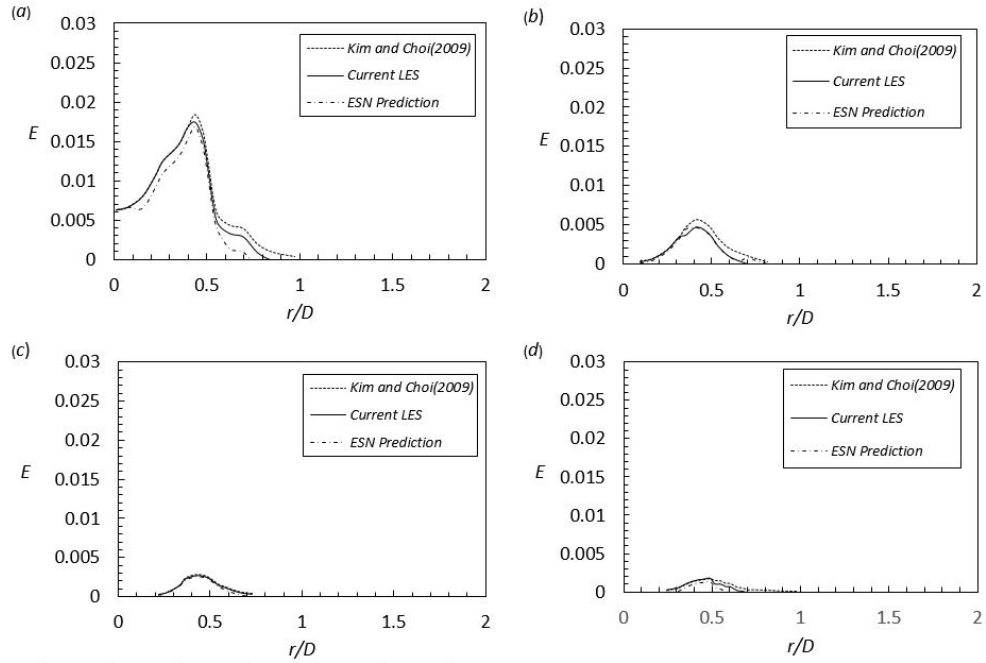

Figure 2.12: Radial distribution of the integrated energy of axial velocity fluctuations Re_D=10^4 at $x/D = 4$, D/θ=50,(a) mode 0 (b) mode 1 (c) mode 2 (d) mode 3.

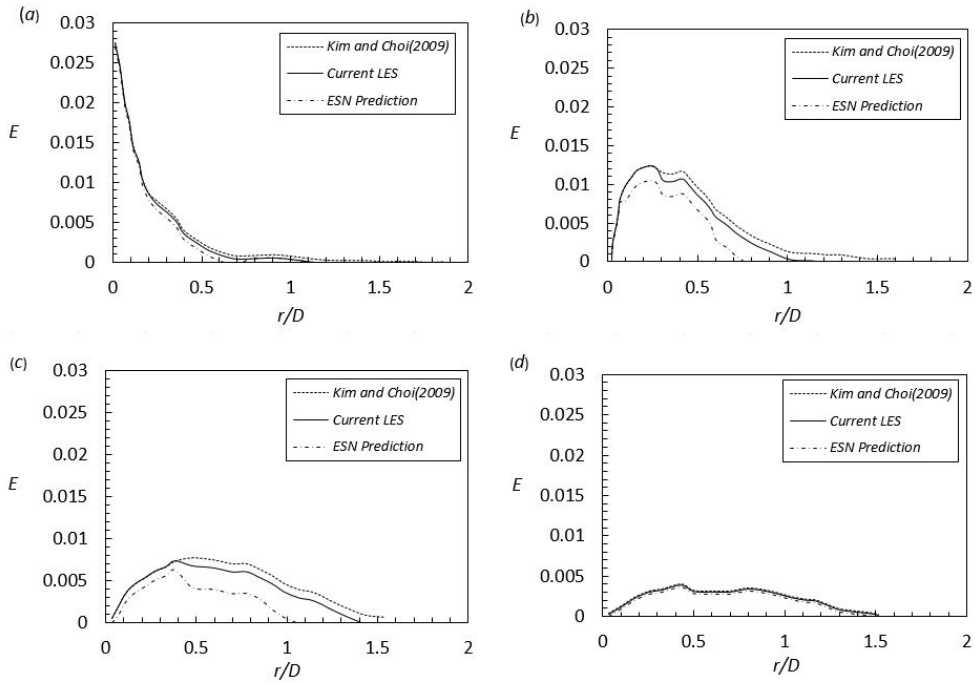

Figure 2.13: Radial distribution of the integrated energy of axial velocity fluctuations Re_D=10^4 at $x/D = 8$, D/θ=50,(a) mode 0 (b) mode 1 (c) mode 2 (d) mode 3.

2.6 Conclusions

An Echo State Network (ESN) has been successfully used to model the short-term dynamic behavior of a turbulent free jet issuing into a quiescent medium. This is the first time ESNs were used to model such a flow field. Based on the results obtained during the course of this study, the following conclusions may be drawn:

- The ESN model quantitatively predicted the mean axial centerline velocity for all Reynolds numbers considered, with a maximum difference between ESN and LES testing results being on the order of 0.02. The ESN was also able to predict the decaying nature of the mean axial centerline velocity.

- The ESN model quantitatively predicted the rms axial velocity fluctuations for all Reynolds numbers considered. The ESN results also displayed the previously observed functional dependence on Reynolds number of the rms velocity fluctuations.

- A parallelized version of the ESN model qualitatively captured the vortical structure

of the jet for a Reynolds number of 3600. Parallelizing the ESN expanded the ability of the model to handle the larger-scale data sets associated with the instantaneous, three-dimensional vorticity field.

- The ESN model predicted the shear layer frequencies for all Reynolds numbers considered. The ESN model was also able to predict the peak frequency of the energy spectra associated with the axial velocity fluctuations. The ESN model predicted a peak frequency value of 0.016 compared to a value of 0.017 obtained from inviscid instability theory.

- The ESN model predicted that the jet-preferred mode would be dependent on the Reynolds number and the momentum thickness. This agreed well with previously published experimental results for Strouhal numbers in the range of 0.3 to 0.6.

- The ESN model predicted that the asymmetric mode [mode 0] was dominant at the jet exit, but past the potential core the double-helix mode [mode 2] became dominant. This was consistent with previously published LES results.

- A limitation of the ESN modeling approach was that as prediction times increased, the Echo State Property of the ESN reservoir resulted in a vanishing driving signal. This loss of signal limits the long-term predictive capability of ESN.

It may be inferred from the above conclusions that ESN provides a viable alternative for modeling the behavior of isothermal, incompressible turbulent jets. Further research is needed to determine if ESNs are equally effective for modeling other turbulent flow fields.

CHAPTER 3

ECHO STATE NETWORKS APPLICATIONS: PREDICTION OF DYNAMICS OF A HEATED TURBULENT JET

3.1 Abstract

The predictive capability of an Echo State Network (ESN) for turbulent flows is explored. An ESN is a particular class of Recurrent Neural Networks (RNNs), proven to model the unsteady behavior of spatio-temporal systems in the past. Two cases of heated turbulent jets discharging from a nozzle are studied. The temperature gradient values considered are 118 and 240 with Reynolds numbers of 8000 and 8500, respectively. LES of the jets are carried out in a commercial CFD software, and the data obtained from LES are used for training and testing the ESN. Detailed comparisons of the mean velocity profiles and the mean temperature profiles along the streamwise and radial directions are provided, along with turbulence quantities. ESN shows a good agreement with LES simulation and the experiment data. The coherent structure of one case is investigated by the visualization of the isosurface of the Q criterion. ESN is shown to be efficient in capturing the vortex rings at the vicinity of the nozzle. Different ESNs are trained and tested for each case, and the hyperparameters used for the vortex prediction are reported. Mean turbulent kinetic energy is studied by simulating three instances with a different temperature gradient. The current study shows a decrease in turbulence with the increasing temperature gradient value. An ESN has the capability to successfully replicate turbulent field behavior based on the results observed in the current study.

3.2 Introduction

The relevance of predicting turbulent flow behavior cannot be overstated, given their prevalence in nature and technical applications. Turbulence has an impact on a variety of phenomena that have been linked to ecological and biological systems. Unfortunately, the sporadic and irregular nature of turbulence complicates its analysis. Turbulence is characterized by its unsteady nature, three-dimensionality, and apparent randomness. The larger integral scales contain most of the kinetic energy, which is then passed to the smaller Kolmogorov scales through the energy cascading process. Beyond this, viscosity prevents the formation of even smaller motions, and the kinetic energy is dissipated into heat which results in a wide range of turbulent length and time scales. All these length and time scales have to be effectively captured to model the turbulent field behavior efficiently. As such, the simulation of such flows is limited by its computational cost. Given the significance of turbulent flows, many studies have been conducted to simulate turbulent flows effectively. The Reynolds-Averaged Navier-Stokes (RANS) equations, the Large Eddy Simulation (LES) method, and Direct Numerical Simulation (DNS) have all been used in the past to describe and simulate turbulent flows. The RANS equations use an averaging technique to the Navier-Stokes equation, which decomposes the flow field into components to be resolved and modeled. This averaging technique requires modeling additional closure terms, namely Reynolds stresses, owing to the fluctuating component, which has resulted in the development of a number of Reynolds stress models. These models are often limited by the physical structure of the flow field. As the complexity of the problem increases, additional equations may need to be solved, increasing computational cost. Yusuf et al. [103] presented an overall review of RANS equations in industrial applications. Another popular turbulence modeling technique is the LES model, in which a filtering operation to the Navier-Stokes equation is used effectively, separating the large-scale eddies from the smaller ones. LES turbulence models, like RANS modeling, seek to resolve the unknown terms in the filtered Navier-Stokes equations, known as Sub-grid Scale stresses. LES mod-

eling provides a broader range of applications and higher solution fidelity, but it comes at a higher computational cost owing to the time step demands and the higher mesh resolution needed to capture flow features. Zhiyin [107] provided a detailed overview and history of using LES to solve complex turbulent flow problems. DNS modeling technique resolves all the turbulent scales ranging from integral scale, associated with the movements carrying most of the kinetic energy to the smallest Kolmogorov scales, thus eliminating the need for any additional turbulence models. Moin and Mahesh [67] provided an overview and difficulties encountered with DNS. Grid resolution and time step requirements for DNS simulations limit its use in engineering applications. DNS is mainly used for academia and research purposes for simple geometries and, along with experiments, is used to develop a fundamental understanding of turbulence.

Variable density turbulent flows can be caused by temperature fluctuations or composition changes in fluids of varying densities [21]. These mechanisms are common in nature and need to be extensively studied to predict different combustion situations. Experiments with heated jets have been documented [77, 84]. Mi et al. [64] investigated the effect of initial conditions on the scalar field of a heated jet at a Reynolds number of 16000. The jets were issued from two different nozzle types, and experiments were performed for both. Anderson and Bremhorst [3] performed heated turbulent jet experiments and reported various turbulent statistics. Self-similarity laws also have been deduced for heated jets from different experiment data for the mean velocity and temperature fields which can be found in Chen and Rodi [24]. Bodony and Lele [10] used LES to predict noise from cold and heated turbulent jets for higher Mach numbers. Similarly, Zhou et al. [108] studied heated turbulent jets at low Reynolds number, investigating the inertia-dominated zone. Smith et al. [87] performed RANS simulation of a heated jet to study the effect of different nozzle shapes on the flow physics. Suto et al [91] simulated four different Reynolds numbers for a heated jet using LES. Significant disparities were found in the near-field scalar fluctuation intensity for the LES and experimental measurements. Colombo et al. [25] performed LES

of a heated jet using FLUENT to measure mean velocity, mean temperature but study of rms temperature fluctuations was missing in this study.

Artificial Neural Networks (ANNs) present an alternative approach to classical turbulent modeling techniques. Artificial neural networks consist of layers of neurons collectively known as nodes. The structure of ANNs is derived from biological neural networks, and they resemble the way real neurons communicate with one another. Each node in an ANN receives one or more weighted input signals, either from the input data or other nodes positioned at a previous network layer, and passes into an activation function. The activation function then calculates the output for the neurons. The model weights are adjusted through a learning algorithm. Based on its use, data flow, structure, activation functions, multiple types of ANNs have been developed. The widely used and effective Recurrent Neural Network (RNN) design, for example, allows for sequential behavior prediction by propagating input from the output nodes. Chaotic time series prediction was carried out using an RNN by both Chandra and Zhang [18] and Diaconescu [30]. However, the training process of RNNs is not without its challenges. Error backpropagation method has been used to train RNNs with some success as underlined in Bishop [9]. According to Chatzis and Demiris [23], one of the method's main drawbacks is that owing to bifurcations, and the training exercise becomes non-converging. Slow convergence and high computational costs of RNNs also limit its utility for practical applications. A significant drawback of RNNs is the vanishing gradient problem which severely limits their ability to learn long data sequences. Despite these challenges, efforts to improve the capability of ANNs continue, and the number of phenomena that ANNs can represent continues to grow. Turbulent flow behavior has been studied using ANNs in the past, which is relevant to our research. In Large Eddy Simulation, Gamahara and Hattori [36] utilized an Artificial Neural Network (ANN) to develop a new sub-grid scale model for modeling the subgrid-scale stresses. ANNs are also used in combustion problems to hasten sub-grid chemistry computations [46, 83]. The relationship between the flow field and the sub-grid scale tensor was

established using a feedforward neural network. Babcock et al. [6] used ANNs to create a controller for decreasing drag in three-dimensional turbulent flows. Mohan et al. [66] utilized ANN architectures to estimate to predict 3D turbulent flows.

Echo State Networks(ESNs) are a particular class of ANNs that have been used in the past to model spatio-temporal systems and address specific issues with RNNs. It was first introduced by Jaeger [47], which together with Liquid State Machines (LSMs) proposed by Maass et al. [62] was unified into a common research area known as "Reservoir Computing." The idea of ESN can be traced back to Neuroscience. Dominey [32] presented an algorithm of the brain, which was the actual precursor of ESN. The readout to the output layer from the reservoir in an ESN is only trained, and the weights of input and recurrent matrices are generated at random. When compared to standard RNNs, this allows for quicker training, minimizing the computational cost of training, which is a significant advantage of ESNs [47]. The reservoir possesses a unique property known as the echo state property, which states that the impact of a previous state or earlier input should fade away as time passes [39]. Tanaka et al [92] presents a thorough examination of current advancements in reservoir computing methods dependent on the structure of the reservoir employed. Utilizing Lyapunov exponent data Pathak et al. [75] used Reservoir Computing to create a model-free approximation for a chaotic system. The author used two unsteady systems, namely, Kuramoto-Sivashinsky (KS) equation and the Lorentz system, to validate their technique. Reservoir computing used for the application of signal processing was studied by Krishnagopal et al. [53], and the findings were found to be superior to the Wiener filter. Turbulent flow counterparts have also been modeled using reservoir computing. The large-scale development of two-dimensional Raleigh-Benard convection was evaluated using Reservoir Computing by Pandey and Schumacher [73]. Rayleigh-Benard convection problem was studied, and temperature fluctuations were predicted using Reservoir Computing by Chang and Lathrop [19]. Kalogirou [51] discuss the use of ANNs in combustion-related engineering problems. Modeling turbulence with ESNs is an alterna-

tive to using traditional turbulence models. The current investigation was prompted by the prior success of utilizing this method.

An Echo State Network was used to model a heated turbulent jet flow (ESN). The ESN data was compared to a validated LES data set and previously published experiment findings to determine the ESN's efficiency. The mathematical equations employed for LES simulation, as well as a review of the computational solution technique and validation of the LES findings, are provided in §3.3. The details of ESN, along with methods used for training and testing the network, are provided in §3.4. The results of this finding that include the centerline flow behavior, vortical structure evolution, and the turbulent kinetic energy distribution are provided in §3.5. The hyperparameters used to train the ESN are also provided in this section. §3.6 outlines the conclusions made from the findings of this investigation.

3.3 LES

The mathematical formulation, computational implementation, and verification and validation of LES results are presented below.

3.3.1 Mathematical Formulation

The governing equations for LES of heated jet flow are the momentum, continuity, and energy equations. The filtered equations are,

$$\frac{\partial \bar{\rho}}{\partial t} + \frac{\partial \bar{\rho}\tilde{u}_i}{\partial x_i} = 0 \tag{3.1}$$

$$\frac{\partial \left(\bar{\rho}\tilde{u}_i\right)}{\partial t} + \frac{\partial \left(\bar{\rho}\tilde{u}_i\tilde{u}_j\right)}{\partial t} = -\frac{\partial \bar{p}}{\partial x_i} + \frac{\partial \bar{\sigma_{ij}}}{\partial x_j} + \rho\bar{g}_i - \frac{\partial \tau_{ij}}{\partial x_j} \tag{3.2}$$

$$\frac{\partial \bar{\rho}\tilde{h}}{\partial t} + \frac{\partial}{\partial x_i}\bar{\rho}\tilde{u}_i\tilde{h} = \frac{Dp}{Dt} + \frac{\partial}{\partial x_i}\left[\frac{\lambda}{c_p}\frac{\partial \tilde{h}}{\partial x_i}\right] - \frac{\partial q_i}{\partial x_i} \tag{3.3}$$

The sub-grid scale model chosen is the popular Dynamic Smagorinsky-Lily model proposed by Germano et al. [38]. The transfer of subgrid-scale turbulent kinetic energy must be accounted to better estimate subgrid-scale turbulence.

3.3.2 Computational Implementation

The numerical case reproduces the experiments H1 and H2 of Anderson and Bremhorst [3], in which a jet of hot air (based on the jet mean jet velocity and diameter) is discharged into cold air in the opposite direction of gravity. The jet comes out of a cubic equation contour nozzle, as shown in figure 3.1.

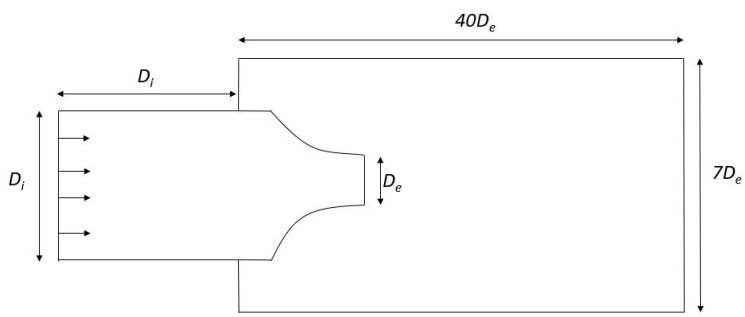

Figure 3.1: Computational domain

Equation 3.4 describes the nozzle radius as a function of length.

$$R = \frac{D_i}{2} - \frac{3}{2}\left(D_i - D_e\right)\left(\frac{x}{L_c}\right)^2 + \left(D_i - D_e\right)\left(\frac{x}{L_c}\right)^3 \tag{3.4}$$

The nozzle dimensions are equal to the ones used in Anderson and Bremhorst [3], in which D_i and D_e are equal to 67mm and 10mm, respectively, and the upstream and downstream straight sections are equal $D_e/2$ and $D_e/4$, respectively. The total length of the nozzle is equal toD_i.

The domain size is based on Kim and Choi [52] simulations, having an outer diameter of $7D_e$ and a downstream length of $40D_e$. The flow inside and outside the nozzle is considered, and a straight section with a length equal to D_i is added upstream of the nozzle, where fully developed profiles from a RANS simulation are applied.

The nozzle inner region is meshed with a minimum spacing of Δr^{+}=2 at walls, forming a structured mesh now with 541 x 138 x 64 cells (in x, r, and θ, respectively).

The nozzle has a zero thickness wall with no-slip boundary conditions applied at both inner and outer walls. Fully developed profiles for x-velocity, turbulent kinetic energy, and turbulent dissipation rate, obtained from a RANS simulation using the Realizable k-ϵ model, are applied at the inlet. Artificial turbulence is generated by the Vortex Method (N = 190 vortices). The pressure inlet and outlet conditions are used at the far-field.

The full scale mesh resolution is shown in figure 3.2.

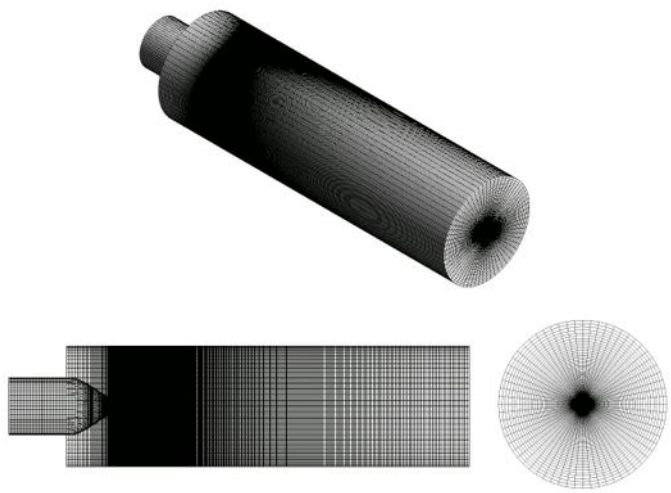

Figure 3.2: Full scale mesh resolution

The numerical methods used in this study are: Fractional Step Method to handle the pressure-velocity coupling, Least Squares to compute gradients, Central Differencing scheme to interpolate convective terms of momentum and energy equation, a second order scheme to interpolate pressure and the Bounded Second Order Implicit to march solution in time, with a fixed time step of $\Delta t = 0.00223 D/U_j$, ensuring a courant number of 0.1. In both cases converged velocity and temperature fields obtained from a RANS simulation are used as initial condition. Instabilities are added to the mean velocity field.

The Central Differencing scheme was used to interpolate convective terms of momentum and energy equations, and a second-order scheme was used to interpolate pressure. The

pressure-velocity coupling was handled using the fractional step approach, and the gradients were computed using least squares. The Bounded Second-Order Implicit was used to march solution in time, with a fixed time step of $\Delta t = 0.00223D/U_j$, ensuring a courant number of 0.1.

3.3.3 LES: Verification and Validation

The grid sensitivity analysis is carried out for the current LES simulation. Three distinct sets of grids, each with 2 million, 4 million, and 8 million cells, are used in the computational grid sensitivity study. For the last two grid sizes employed, the mean axial profiles of velocity and temperature are compared. The profiles obtained do not vary, thus indicating a mesh-independent solution. As a result, 4 million cell grid was employed in this research.

3.4 ESN

An input vector $u(t)$ of size K units is supplied to a dynamic 'Reservoir' with N units. The reservoir is linked to an N_y output layer $y(t)$. The reservoir takes input at discrete time t and combines its state to generate output at time t+δt.
Echo State Networks use an RNN with leaky -integrated discrete-time continuous-value units [61]. The update equations for an ESN are

$$\widetilde{x(n)} = \tanh(W^{in}[1; u(n)] + Wx(n-1)) \tag{3.5}$$

$$x(n) = (1-\alpha)x(n-1) + \alpha\widetilde{x}(n) \tag{3.6}$$

where $x(n)$ represents neuron activations of reservoir and $\widetilde{x(n)}$ are its update at every time step n. tanh() function is used as the sigmoid wrapper and is one of the most common choices. $\alpha \in$ (0,1] is the leaking rate, [;] represents a vertical vector (or matrix) concatenation , W^{in} and W are the input weight matrix and recurrent weight matrix respectively [61]. Once the reservoir is trained, the output weight matrix is generated using linear re-

gression. The linear readout layer is defined as,

$$y(n) = W^{out}[1; u(n); x(n)] \tag{3.7}$$

3.4.1 Pseudo algorithm

The ESN described originally in Jaeger [47] can be briefly summarised as,

- The weights of input matrix and recurrent matrix are generated at random.
- The activation of reservoir units is collected using equation 4.6 once the inputs $u(n)$ are supplied to the network.
- The output weight matrix is calculated by minimizing the error between the predicted and desired output using a linear readout layer.
- Once the network is trained, the output to any unseen test data can be calculated.

3.4.2 ESN Training

The LES data set was split into two groups for each Reynolds number, one for training and the other for testing. The ESN reservoir was fed the training data set, which subsequently generated the ESN's initial output. The error associated with the ESN output was determined by comparing the ESN's initial output to the training data set. The mean square error between the ESN's initial and target output obtained from the training set was reduced.

$$E(y, y^{t\arg et}) = \frac{1}{N_y}\sum_{i=1}^{N_y}\sqrt{\frac{1}{T}\sum_{n=1}^{T}\left(y_i(n) - {y_i}^{t\arg et}(n)\right)^2} \tag{3.8}$$

where E is ther training error, N_y denotes the size of output dimensions, T is the number of training samples, y_i is the data predicted by ESN, and y_i^{target} is the target output.

3.4.3 ESN Testing

As previously stated, the resultant LES data set was split into two unique groups for each Reynolds number, one for training and the other for testing. Once the training is complete, the ESN model autonomously predicts the turbulent jet's future flow behavior. The so-called LES testing data set was utilized to evaluate the efficacy of the ESN model predictions.

It's worth noting at this time that the ESN reservoir's Echo State Property prevents longer-term prediction of turbulent jet behavior. This is due to the fact that the driving signal to the reservoir will diminish in amplitude with time. It has been known from Lorentz [58] fundamental work that longer-term prediction of chaotic behavior is impossible. Because turbulent flows are inherently chaotic, longer-term flow predictions are impossible. Thus the Echo State Property does not necessarily reduce the efficacy of the ESN method.

3.4.4 ESN Parallel Implementation

Another shortcoming of the ESN technique is the reservoir size limitation. The computational cost of adjusting the hyperparameters rises as the number of nodes in the reservoir grows, extending the time required to create a functional model that correctly predicts flow field behavior. For the vast majority of the predictions generated throughout this research, this was not an issue. The number of neurons required to forecast the turbulent vorticity field, i.e., the Q-criterion, became prohibitive. ESN was used in parallel mode to solve this issue.

The flow field was divided into multiple spatial regions for the parallel execution of the ESN model. A distinct ESN reservoir predicts each spatial region. The concept of the locality parameter is used to create continuity between two adjacent spatial regions in the flow field. During training, each reservoir evolves in parallel, generating a unique set of output weights. Pathak et al. [74] successfully utilized this technique to predict the dynamics of the Kuramato-Shivansky equation.

3.5 Results

Two heated jets used in the experiment of Anderson and Bremhorst [3] is simulated, and the results are compared to the prediction from the ESN. The details of the simulation are summarized in table 3.1.

Table 3.1: Simulation details

	U_j	ΔT	Re	Fr
Case 1	22.4	118	8000	13200
Case 2	35.8	240	8500	16000

Here, U_j and ΔT_j denotes the nozzle velocity and the temperature gradient between the jet temperature and the ambient temperature, respectively. The full-scale ESN is run for Case 1, and the unsteady vortical structures are predicted using the parallel architecture of ESN as described in §3.4 previously. The mean properties of temperature and velocities are also compared. Data from LES is used for training and testing. LES simulation is carried out for a total of 3s, and the training length used is 2.2 seconds. The rest of the data are used for testing purposes. Different sets of hyperparameters are used in both of these cases. The hyperparameters used for in this study are summarised in table 3.2.

3.5.1 ESN Hyperparameters

A list of hyperparameters used in this study is given in table 3.2. For the two cases simulated in this study, separate hyperparameters were used. A grid search was employed to tune the parameters used for prediction.

3.5.2 Mean velocity and temperature

The results obtained from the LES simulation and the one predicted by ESN are compared with the decay laws obtained by Chen and Rodi [24] for the mean properties along the

Table 3.2: Hyperparameters used in this study

Hyperparameters	Case 1	Case 2
Leak rate	0.2	0.1
Size of reservoir	1000	1000
Regularization coefficient	1e-07	1e-08
Probability of non-zero connections	0.15	0.2
No of groups	200	-
Locality parameter	2000	-

centerline. The equations derived by Chen and Rodi [24] along the centerline of a jet are,

$$\frac{U}{U_j} = 6.3 * \sqrt{\frac{\rho_j}{\rho_o}} * \frac{d}{x} \tag{3.9}$$

$$\frac{\Delta T}{\Delta T_j} = \frac{T - T_o}{T_j - T_o} 5.4 * \sqrt{\frac{\rho_j}{\rho_o}} \frac{d}{x} \tag{3.10}$$

In equations 3.9 and 3.10, U, T, U_j, T_j, T_o denote the centerline velocity, centerline temperature, jet velocity, jet temperature and ambient temperature respectively.

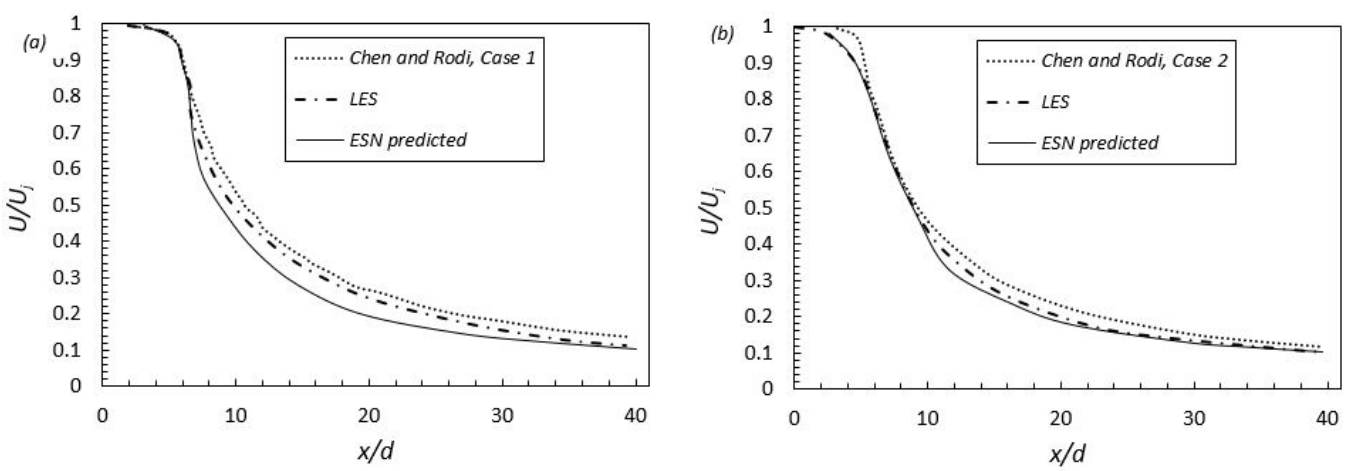

Figure 3.3: Mean axial velocity along the centerline normalised by the jet velocity, (a) Case 1 (b) Case 2

The mean axial velocity along the centerline are compared for both cases, and a reasonable agreement was achieved with the decay laws derived by Chen and Rodi [24]. ESN

captured the decay of the stream-wise velocity with a minor difference in magnitude. The discrepancy between the decay law and the LES simulation can be attributed to the fact that the decay laws do not hold in the near vicinity of the jet. The decay laws yield a value of infinity for the velocity ratio as the length approaches zero. This has already been observed in the investigations of Wang et al. [96] and Foysi et al. [35].

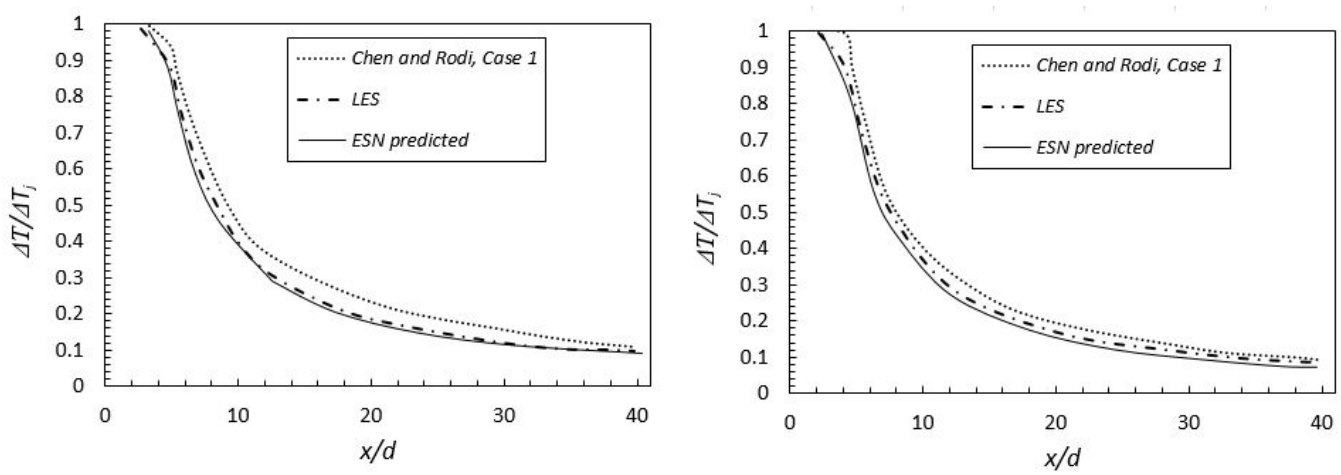

Figure 3.4: Mean axial temperature along the centerline normalised by the jet velocity, (a) Case 1 (b) Case 2

Other factors affecting the results could be the jet inflow conditions like the jet momentum thickness as observed in Kim and Choi [52]. In general, the ESN successfully captured the centerline decay of the mean velocity and mean temperature along the stream-wise direction. Similar profiles were also obtained by Roger et al. [81] in their LES study conducted in OpenFoam.

The radial profiles for the mean velocity and mean temperature are compared with the experimental fit data. In Anderson and Bremhorst [3], the equation used to fit the radial profile is given by

$$\frac{U}{U_c} = exp\left[a\left(\frac{r}{x}\right)^b\right] \tag{3.11}$$

This equation was developed by Gehrke [37]. The coefficients for equation 3.11 are given in Anderson and Bremhorst [3], where the values are a=-34.478 and b=1.7282. The results from LES and ESN are compared to the Gaussian profile. Various streamwise locations are

used to observe the self-similarity profile.

In figures 3.5, 3.6 and 3.7, the mean radial velocity at different streamwise location are shown and self-similar behavior was observed. Only case 2 is shown here, as a line of best fit is added to case 2 data in Anderson and Bremhorst [3] as well as Roger et al. [81]. The pseudo-similarity is further illustrated here, which was observed by Foysi et al. [35] in the numerical simulation of Helium jets. The ESN captured this behavior, and the data compared well with the experiment and the gaussian fit.

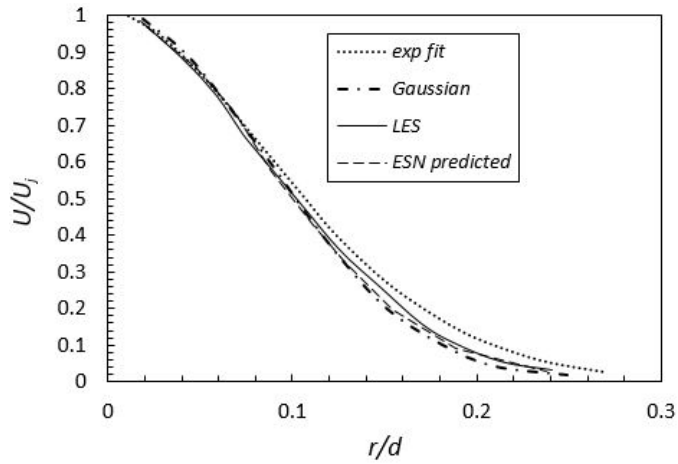

Figure 3.5: Mean radial velocity normalised by the jet centerline velocity at $x/d = 10$ for case 2

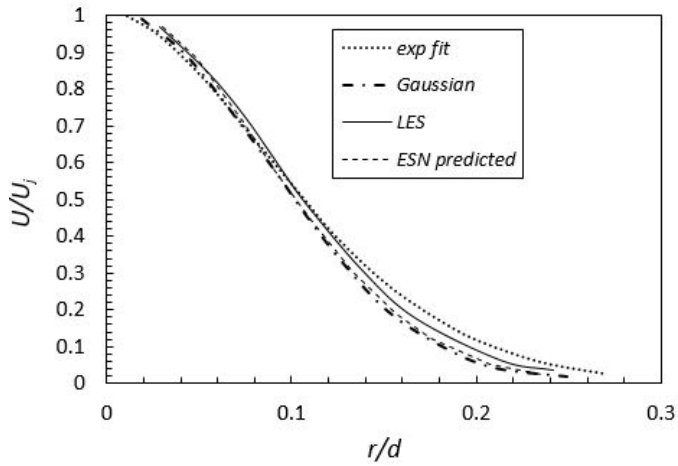

Figure 3.6: Mean radial velocity normalised by the jet centerline velocity at $x/d = 20$ for case 2

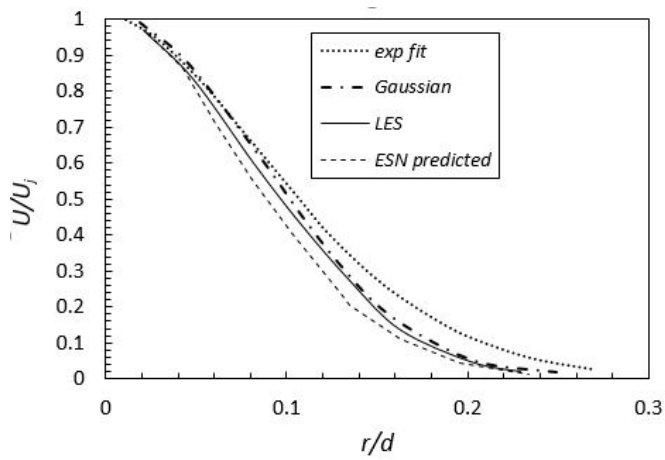

Figure 3.7: Mean radial velocity normalised by the jet centerline velocity at $x/d = 40$ for case 2

Similar behavior was seen for the temperature profile. The mean radial temperature at various streamwise locations are compared with the gaussian and experiment fit data. The same equation 3.11 was used to obtain the line of best fit for the experiment data but with different coefficients where a=-28.9205 and b=1.7871.

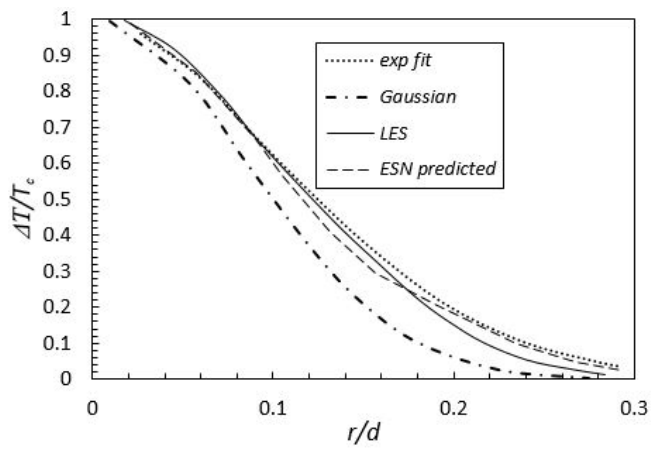

Figure 3.8: Mean radial temperature normalised by the jet centerline temperature at $x/d = 10$ for case 2.

In figures 3.8, 3.9 and 3.10, the mean radial profile of temperature normalised by the centerline temperature are shown. The ESN underpredicted the profile, but the self-similarity behavior was well captured.

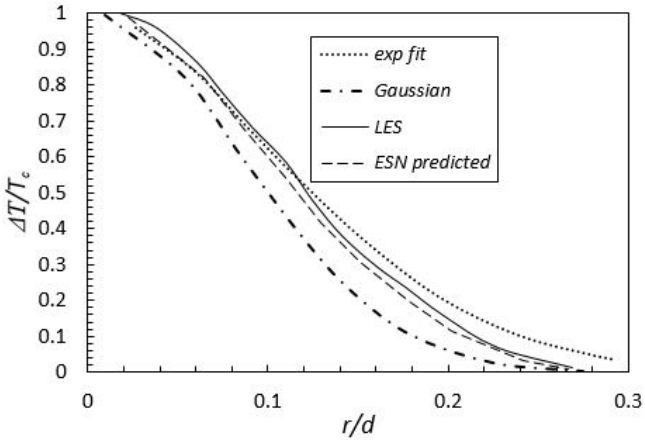

Figure 3.9: Mean radial temperature normalised by the jet centerline temperature at $x/d = 20$ for case 2.

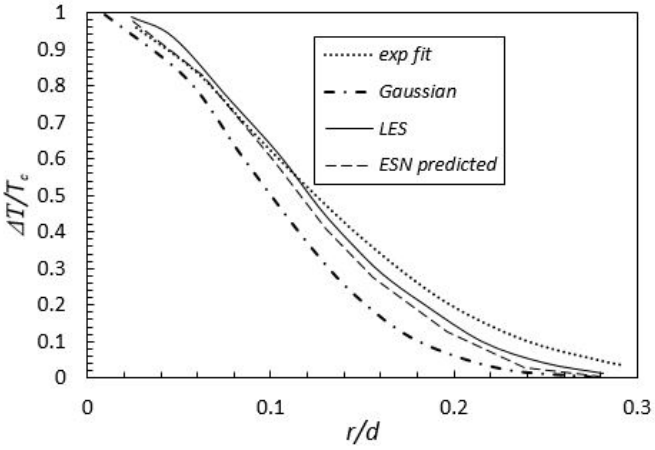

Figure 3.10: Mean radial temperature normalised by the jet centerline temperature at $x/d = 40$ for case 2.

3.5.3 Turbulent quantities

The rms velocities along the radial direction and different streamwise locations are measured. The rms velocity and the rms temperature have similar evolution as the jets are very similar. The data agreed well with the experiment by Anderson and Bremhorst [3] and the simulations by Wang et al. [96]. There seemed to be some discrepancy in terms of the magnitudes, but the trend was well predicted.

The rms temperature fluctuations at the centerline normalized by the temperature gradient are shown in figure 3.11. Again, the ESN captured the fluctuating nature of turbu-

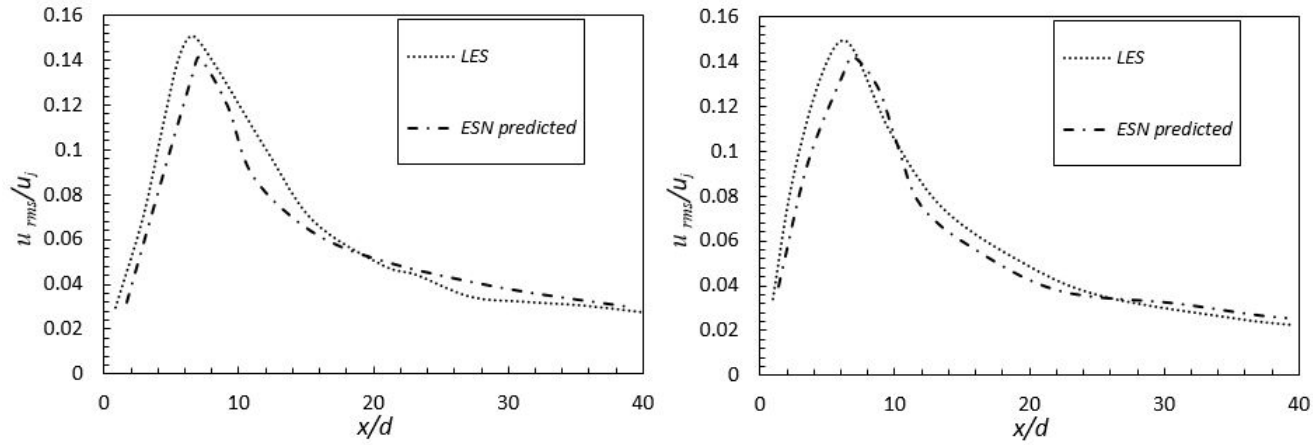

Figure 3.11: rms of axial velocity fluctuations normalised by jet velocity, (a) Case 1 (b) Case 2.

lence.

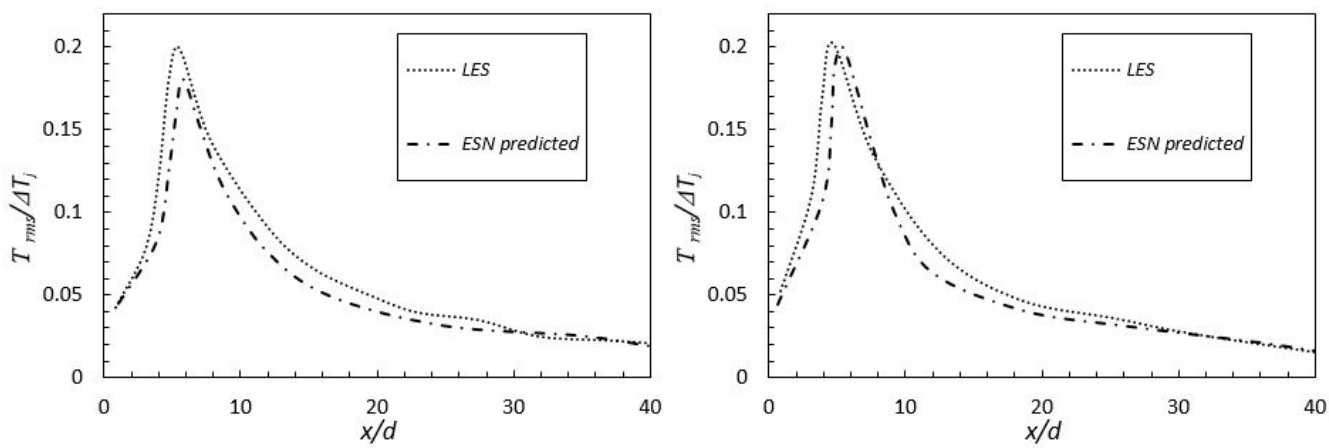

Figure 3.12: rms of temperature fluctuations at the centerline normalised by temperature gradient, (a) Case 1 (b) Case 2.

For case 2, the radial and streamwise profiles of the rms fluctuations are shown and compared with experimental data fit. The equations are provided by Roger et al. [81].

$$\frac{u'^2}{U_c^2} = a_1 \left(\frac{r}{x}\right)^2 exp\left[b_1 \left(\frac{r}{x}\right)^2 +\right] c_1 exp\left[d_1 \left(\frac{r}{x}\right)^2\right] \tag{3.12}$$

$$\frac{v'^2}{U_c^2} = a_2 exp\left[b_2 \left(\frac{r}{x}\right)^{c_2}\right] \tag{3.13}$$

The various coefficients for equations 3.12 and 3.13 are given by Anderson and Bremhorst [3]. The coeffiecients are a_1=1.6139, b_1=-92.9937, c_1=0.22, d_1=-53.975, b_2=-99.9935, a_2=-0.0349 and c_2=2.1931. The data predicted by ESN matched well with the experimental fit data.

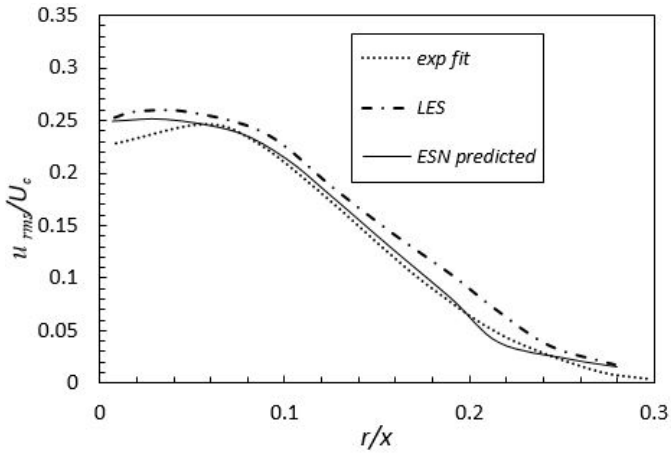

Figure 3.13: radial profile of rms axial velocity normalised by mean centerline velocity, $x/d = 10$.

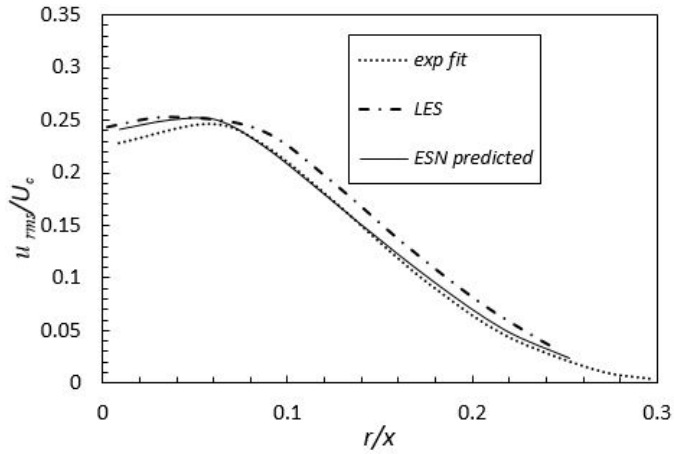

Figure 3.14: radial profile of rms axial velocity normalised by mean centerline velocity, $x/d = 20$.

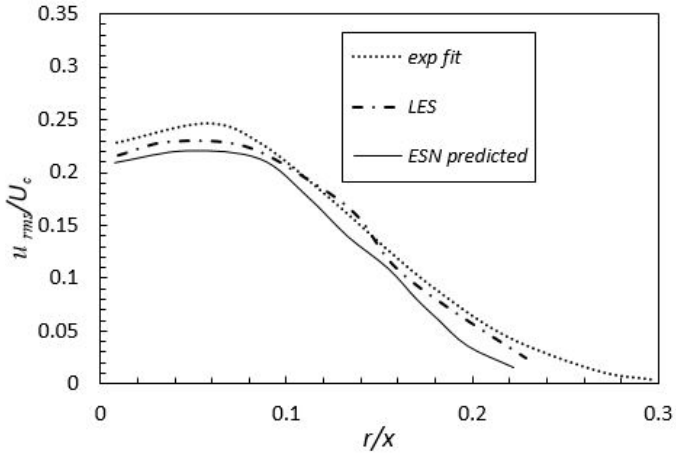

Figure 3.15: radial profile of rms axial velocity normalised by mean centerline velocity, $x/d = 40$.

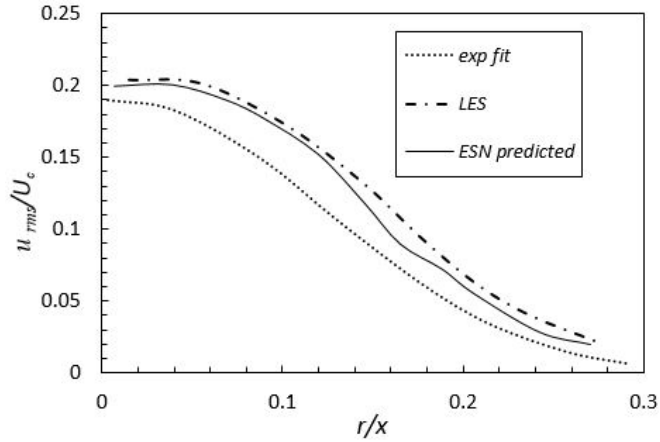

Figure 3.16: radial profile of rms radial velocity normalised by mean centerline velocity, $x/d = 10$.

3.5.4 Turbulent kinetic energy

To study the effect of temperature gradient on the mean turbulent kinetic energy, three different cases are simulated as shown in table 3.3. The mean turbulent kinetic energy plot is shown in figure 3.19.

As reported in Anderson and Bremhorst [3], turbulence increases due to density variation as a result of the mixing of gases. However, the turbulence level decreases due to an increase in temperature gradient values. The mean turbulent kinetic energy decreased with the increasing temperature gradient, which is well captured by the ESN. This has also

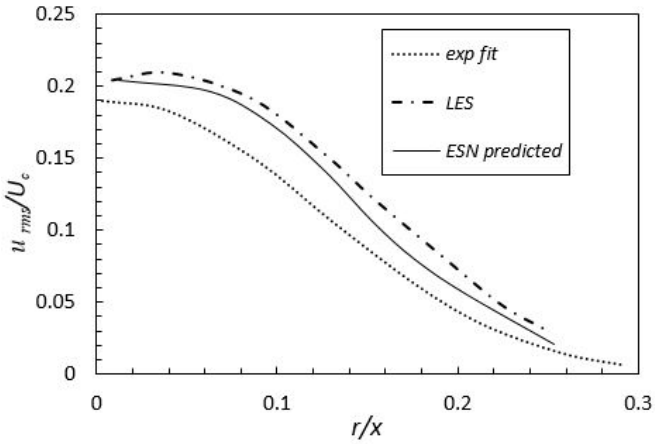

Figure 3.17: radial profile of rms radial velocity normalised by mean centerline velocity, $x/d = 20$.

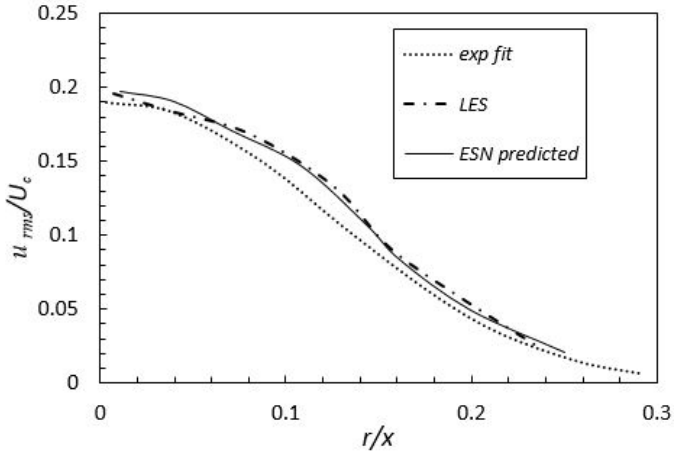

Figure 3.18: radial profile of rms radial velocity normalised by mean centerline velocity, $x/d = 40$.

been reported by Roger et al. [81].

3.5.5 Vortical Structure

The vortical structure obtained from the LES simulation is compared with the structure predicted by ESN in figure 3.20. The vortex rings formed near the jet exit, and the nozzle vicinity and the large-scale structures developed as the flow moved further away from the nozzle. This behavior is due to the Kelvin-Helmholtz instability. Large scale structures formed due to vortex pairing as the shear layer became unstable at the jet exit. The Q-criterion is plotted to visualize the coherent structures of the jet, and the vortical structure

Table 3.3: Simulation details

	U_j	ΔT	Re	Fr
Case 1	22.4	118	8000	13200
Case 2	22.4	236	5300	65000
Case 3	22.4	354	3800	4300

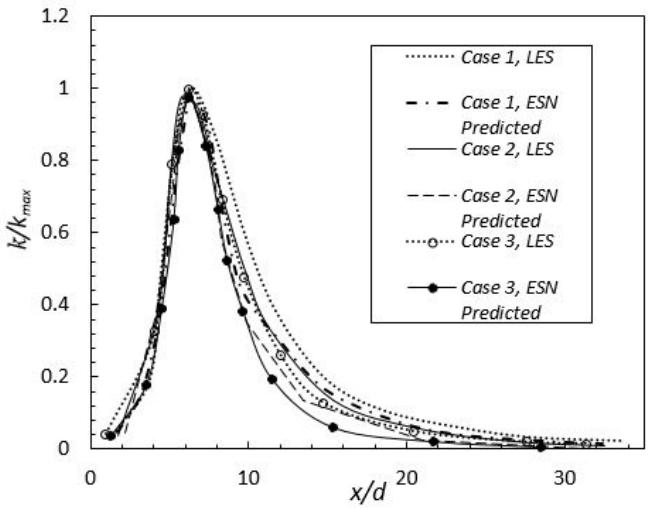

Figure 3.19: mean turbulent kinetic energy normalised by the maximum kinetic energy along the centerline for the three jets.

predicted by ESN was in good agreement with the LES data set.

3.6 Conclusion

An ESN has been used to model a hot jet issuing from a nozzle into cold air in the opposite direction of gravity. The following conclusions were drawn based on the current based on the current observations:

- The ESN model predicted the decaying nature of mean centerline velocity and mean centerline temperature. The maximum difference observed between the decay laws and ESN's results were on the order of 0.03. The ESN model also captured the self-similarity behavior of the mean axial velocity distribution along the radial direction.

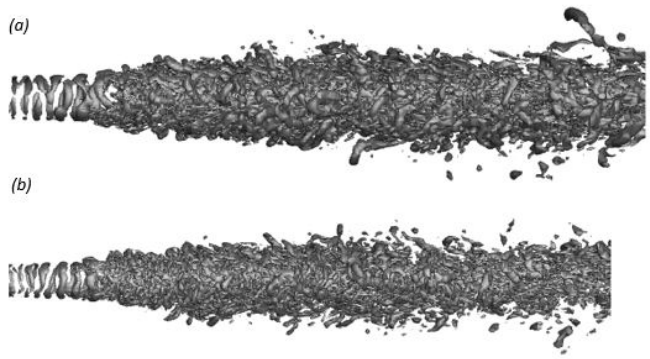

Figure 3.20: Instantaneous vortical structure for Case 1 (a) LES (b) ESN prediction. Shown are the Q criterion at a Q value of 75000.

- The ESN model correctly predicted the mean axial velocity and temperature fluctuations along the jet. The ESN model also correctly calculated the peak values of turbulent intensities for both cases considered in this study. The ESN was used to measure the radial velocity fluctuations along different streamwise locations for Case 2 and demonstrated an excellent agreement with the experiment fit data.

- The parallel architecture of the ESN was used to capture the vortical evolution of the jet at a Reynolds number of 8000, and a good qualitative agreement with the simulation was obtained. The capacity of the model to handle larger-scale datasets related with the instantaneous, three-dimensional vorticity field was improved by parallelizing the ESN.

- The ESN model correctly predicted the decreasing nature of mean turbulent kinetic energy with increasing temperature gradient value. This was consistent with previously published LES results.

- One of the limitations of the ESN model was its inability to predict long data sequences. The driving signal to the reservoir vanishes over time which limits the predictive capability of ESN.

Based on the conclusions, the ESN has proven valuable to model heated turbulent jet be-

havior. Additional investigation of turbulent flow fields with an ESM is required to determine its effectiveness.

CHAPTER 4

MACHINE LEARNING APPLIED TO THE PREDICTION OF THE FLUID DYNAMICS OF VARIABLE DENSITY TURBULENT JETS

4.1 Abstract

The efficiency of utilizing an Echo State Network (ESN) to estimate turbulent flow field features is investigated. ESNs are a kind of Recurrent Neural Network that can capture the transitory nature of a spatiotemporal system without having to solve the fundamental mathematical equations. A variable density jet originating from a cylindrical tube that passes through a weakly restricted co-flow of low-speed air streams is used. According to the findings, this is the first time an ESN has been used to model variable-density jets. Three cases of jets, i.e., Helium-air jet, air-air jet, and CO_2-air jet with Reynolds numbers of 7000, 21,000, and 32,000, respectively, are compared to previously reported turbulent flow results. ESN training is carried out with the help of a validated LES dataset obtained from commercial CFD software. To see how successfully the ESN predicted flow field behavior, a different LES dataset is used. A hyperparameter search is conducted to enhance the ESN's capacity to forecast the turbulent flow field under consideration. Compared to LES model data and previously published experimental data, the ESN model is able to reproduce turbulent flow field statistics. The statistical results seem to confirm the faster development of lower-density jets compared to heavier jets when identical exit momentum flux is used. In addition to this, ESN is able to capture the large vortex rings formed at the jet exit for the Helium jet formed due to the Kelvin-Helmholtz instability. Based on the findings of this investigation, it is evident that an ESN can effectively model turbulent flow fields.

4.2 Introduction

Turbulent flows often occur in natural and industrial systems, necessitating a detailed study. Turbulence has a significant effect on a range of phenomena associated with environmental and biological systems. The prediction of turbulent flow is crucial in the design of technical devices. However, turbulent flow is highly chaotic, three-dimensional, and unsteady. Turbulent flows consist of various scales ranging from the largest integral scales to the smallest Kolmogorov scales. Most of the kinetic energy is contained in the largest scales. Through an inertial process, this energy is cascaded to the smallest scales beyond which viscous dissipation of kinetic energy into heat results in a variety of time and length scales that must be represented to predict turbulent flows accurately. As a result, the computing expense of modeling turbulent flows limits the realistic prediction of flow properties. Given the significant nature of turbulent flow prediction, considerable study has been conducted to model them successfully.

The modeling of turbulent flows has historically involved the use of turbulence models like Direct Numerical Simulation (DNS), Large Eddy Simulation (LES), and Reynolds-Averaged Navier-Stokes (RANS). RANS equations are time-averaged fluid flow equations that decompose an instantaneous quantity into its time-averaged and fluctuating components. This averaging method introduces new terms known as Reynolds stresses into the equation, which must be modeled. Several turbulence models have been used to generate a closed system of equations in the past. The physical state of the problem often constrains the applicability of these models. Additionally, RANS models are often constrained by the modeling assumptions established in the model's mathematical formulation. Yusuf et al. [103] discussed the use of RANS modeling in terms of industrial applications. Speziale [88] addressed the applicability of RANS combined with LES to solve complex flow problems. LES technique uses a filtering operation that effectively separates the larger eddies from the smaller eddies. The larger eddies can be directly resolved, whereas the smaller eddies, which tend to be isotropic, should be modeled using sub-grid scale models. While LES

modeling expands the potential application and fidelity of the solution, it does so at the expense of increased computational cost due to the time step requirements and increased mesh resolutions. The uncertainties associated with the sub-grid scale models for some flow problems also limit its use. Zhiyin [107] provided a detailed history of the application of LES for turbulent flows. In DNS, the Navier-Stokes equations are solved directly without any modeling assumptions. It entails solving a whole range of temporal and spatial scales associated with a turbulent flow, from very large scales down to the Kolmogorov length scale. Moin and Mahesh [67] discussed the applications and challenges of DNS. Although DNS is the most accurate way of modeling turbulent flows, the mesh size and time step requirements limit its application for industrial engineering flows. Hence, it is only used to solve simple geometries and aid in understanding turbulent flows.

Variable density turbulent flows, caused by temperature differences triggered by reactions or changes in composition caused by fluids of varying densities, are expected in nature and technical systems. Modeling the dynamics of such flows and forecasting turbulent combustion conditions requires predicting turbulent mixing in flows with changing densities. Variable density jets have been the subject of very few investigations. Ahmed et al. [1] conducted an experiment in which an air/helium combination was discharged into a swirling flow. Sreenivasan et al. [89] and Kyle and Sreenivasan [54] investigated experiments on circular jets of various densities made by premixing helium and air. Monkewitz et al. [69] and Monkewitz and Pfizenmaier [70] conducted additional entrainment and mixing tests in transitional jets where varied densities were created by heating the air. Panchapakesan and Lumley [72] conducted an experiment in which helium was injected into open quiescent air via a round jet. Djeridane et al. [31], Amielh et al. [2], and more recently Boujemaa et al. [12] conducted experiments on helium, air, and carbon dioxide departing into low-speed air co-flow. For round jets with three distinct density ratio values, the LES performed by Wang et al. [96] provides a detailed comparison between experimental and numerical research. In their numerical investigation, they duplicated the experiment

of Amielh et al. [2] and Djeridane et al. [31]. In Jenkins and Goldschmidt [48], Davies et al. [28], Bashir and Uberoi [7], Antonia et al. [4], Browne et al. [14] and Ramaprian and Chandrasekhara [79], only mildly heated jets with density ratios between 0.8 and 0.9 were considered for plane jets. The evolution of the jet does not alter much as a result of these values. Foysi et al. [35] also performed numerical analyses for plane jets with various density ratios, obtaining good agreement between experiments and numerical studies, and providing additional insight into the round-jet/plane jet anomaly Pope [78]. In variable-density flows, the occurrence of global instability is also a significant phenomenon. The variable density jets evolve in the same way as the constant density jets above a value of 0.5-0.6, according to Kyle and Sreenivasan [54], Monkewitz [68], Raynal et al. [80], Hallberg andStrykowski [41], Lesshafft et al. [56] and Nichols et al. Variable density jets tend to have high energy near the shear layer, placing a higher demand on grid intensity, making LES difficult.

Artificial Neural Networks (ANNs) provide a new technique for turbulence modeling. ANNs are computer counterparts of biological neurons that can be used to predict the behavior of chaotic systems. ANNs are made up of layers of nodes interlinked to one another. The nodes combine the data from input nodes, and other nodes with a set of weights passed through an activation function to the output layers. The weights of ANNs are updated through a learning algorithm which is another important factor influencing their success. Various types of ANNs are available depending upon their architecture, the number of nodes, types of activation function used. For instance, Recurrent neural networks (RNNs) are neural networks that cycle past outputs back to the network as inputs while maintaining hidden states. Woolley et al. [99] used ANNs in combination with other techniques like NARMAX to predict nonlinear behavior of chaotic systems, citing Lorentz system as an example. Similarly, Zhang [106] predicted sunspot time series using ANNs. Chandra and Zhang [18] and Diaconescu [30] used neural networks for time series data. They used chaotic time-series data to train Elman recurrent neural networks. They utilized

the Mackey-Glass, Lorenz, and Sunspot time series to illustrate the cooperative neuro-evolutionary techniques' performance and found that they outperformed other methods in terms of accuracy. Han et al. [42] utilized a recurrent predictor neural network (RPNN) with linear nodes to model and forecast chaotic time series. The neural network was trained using a back-propagation through time (BPTT) learning method. Vlachas et al. [95] suggested the use of Long Short Term Memory (LSTMs) neural networks for predicting high-dimensional chaotic systems. For all systems studied, it seemed to outperform Gaussian Processes (GPs) in short-term predicting. Although RNNs have been used successfully in the past, their use is still limited. Slow convergence and high computational costs of RNNs limit their utility for practical applications. A significant drawback of RNNs is the vanishing gradient problem which restricts their ability to learn long data sequences. Despite these challenges, attempts to extend the potential of ANNs continue, as does the range of phenomena represented by ANNs. ANNs have already been used to simulate turbulent flows, which is relevant to our research. Yuhong and Wenxin [102] predicted the friction factor of an open channel flow and compared it to the empirical formula achieving a reasonable agreement. Babcock et al. [6] used a neural network to train a function that is almost similar to an analytically determined control rule. They showed a neural controller's capacity to maintain a drag-free flow in a completely chaotic fluid simulation. ANNs are also utilized to accelerate sub-grid chemistry calculations in combustion issues [46, 83]. Echo State Networks (ESNs) are a subclass of ANNs that have previously been used to simulate spatiotemporal systems and tackle particular challenges with RNNs. Jaeger [47] introduced the concept of ESN as a modification of RNN where only the output weights of the network are modified through a learning algorithm. Maass et al. [62] presented Liquid State Machines(LSMs) as a computational tool to model biological neural networks. Later, the concepts of ESN and LSM were merged into a common research area dubbed 'Reservoir Computing.' ESNs offer a significant advantage over traditional RNNs, as only the output weights are learned through training, and the weights of the input matrix and re-

current matrix remain fixed. Dominey [32] proposed an algorithm for the brain that served as the foundation of ESN. While ESNs are simple to comprehend and computationally cheap, they need considerable experience to build effectively. Numerous global hyperparameters must be adjusted to deploy the ESN effectively. Application of ESN so far include speech recognition [86], robot control [5], forecasting financial market [57] and dynamical systems such as the Mackey-Glass system [63]. Echo state networks have a unique feature known as the 'echo state property.' It states that as time passes, the influence of a former state or previous feedback can fade away on the future state [39]. ESNs in the current literature have been found to use three configurations while predicting chaotic behaviors, namely, observer mode (or non-autonomous mode) where model free prediction is achieved with limited state variables [60], the feedback (or autonomous) mode in which during the prediction the output of a previous timestep is fed as the input in the reservoir [59, 75] and finally custom ensemble methods where ESNs are used in conjunction with knowledge-based models [74]. Tanaka et al. [92] provides an in-depth analysis of recent advances in reservoir computing methods for several types of reservoirs. Several studies have been performed to understand the dynamics of Reservoir computations to enable effective prediction of dynamic systems. Carroll [15, 16, 17] used RC-ESN at the edge of chaos to perform predictions and concluded that it does not necessarily improve the performance. A study in the sensory phase with two parallel reservoirs was performed by Zhang et al. [105] and concluded that parallel reservoirs are limited in collecting dynamics of a coupled chaotic system of the entire system in the long run. Turbulence has also been studied using Reservoir Computing. Chang and Lathrop [19] used Reservoir Computing to study temperature fluctuations in a Rayleigh-Benard convection problem. Turbulence modeling using ANNs and ESNs is a viable alternative to conventional turbulence models. The present study was motivated by previous success with this approach.

ESN was used to study the flow behavior of three distinct variable-density jets. The ESN results were compared to a validated LES dataset and previous experiments to explore

its effectiveness. The computational method used, grid sensitivity study, along with the mathematical equations used for LES, are provided in §4.3. The details of ESN, as well as the training and testing procedure, are explained in §4.4. Results of the current study that include the analysis of mean flow properties, turbulence quantities, the study of the Reynolds stresses, and coherent structures of the jet are provided in §4.5. Finally, the conclusions of the present study are outlined in §4.6.

4.3 Large Eddy Simulation

Large Eddy Simulation (LES) of three variable density jets issuing from a straight tube into a low-speed so-flow is carried out, and the data obtained is used for training and testing the Echo State Network (ESN).

4.3.1 Mathematical Formulations

The low mach number version of the filtered compressible Navier-Stokes equation is solved for the mass, momentum, energy, and species transport equations. The low mach-number versions of these equations as shown in Wang et al. [96] are as follows:

$$\frac{\partial \rho}{\partial t} + \frac{\partial \rho u_i}{\partial x_i} = 0 \tag{4.1}$$

$$\frac{\partial \rho u_i}{\partial t} + \frac{\partial \rho u_i u_j}{\partial x_j} = \frac{1}{Re}\frac{\partial \tau_{ij}(\mu)}{\partial x_j} - \frac{\partial P^1}{\partial x_i} \tag{4.2}$$

$$\frac{\partial \rho c}{\partial t} + \frac{\partial \rho c u_j}{\partial x_j} = \frac{1}{ReSc}\frac{\partial \tau_{ij}(\mu)}{\partial x_j} - \frac{\partial P^1}{\partial x_i} \tag{4.3}$$

$$\rho = F(P^{(0)}, T, c) \tag{4.4}$$

where c, Sc are the mass fraction of the jets and Schmidt number respectively. P^1 is the dynamic pressure related to the momentum field, and P^0 is the thermodynamic pressure

associated with density and temperature. The filtering operation is carried out for these equations, and filtered LES equations are obtained. Dynamic Smagorinsky model is used to account for the subgrid scales effect.

4.3.2 Computational Implementation

Figure 4.1 depicts the computational model that was used in this study. Three jets (Helium/Air, air/air, and CO_2/air) are discharged from an inner pipe, of diameter D_j, into a low-speed air stream inside an outer pipe of diameter D_e. The domain used here is the same as used by Wang et al. [96]. The parameters used for various jets are shown in table 4.1.

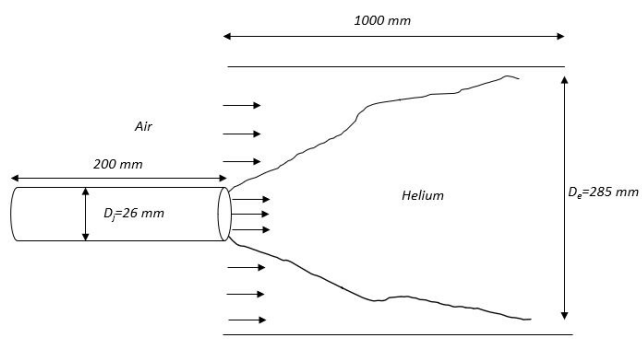

Figure 4.1: Computational domain used for LES.

Kim and Choi [52] grid spacing's recommendations for LES are $\Delta x^+ = 50 - 150$ and R_j $\Delta\theta^+ = 15 - 40$, where is the equal to $D_j/2$. In the x-direction, an averaged spacing of $\Delta x^+ \approx 50$ is used, leaving 278 cells from the jet exit to the downstream end of the domain. Wang et al. [96] used 462 grid points to cover the same region. In the azimuthal direction a value of R_j $\Delta\theta^+ \approx 15$ is used, resulting in 64 grid points. In the radial direction 154 cells are used, in which 34 cells covered the jet radius.

Cells are clustered in axial and radial directions to catch the boundary and shear layers fully. Therefore, minimum spacings of $\Delta x^+ \approx 15$ and $\Delta r^+ \approx 2$ are used at $x = 0$ and $r/D_j = 0.5$, respectively. At the outer pipe wall ($r/D_j = 0.5$), a minimum spacing of $\Delta r^+ = 2$, based on the airstream inlet Reynolds number, is used to catch the boundary layer fully. The mesh resolution in the z-plane is shown in figure 4.2.

Table 4.1: Parameters used for jet.

Jet	ρ_j/ρ_e	U_j	U_e	Re_j
Helium	0.14	32	0.9	7000
Air	1	12	0.9	21,000
CO_2	1.52	10	0.9	32,000

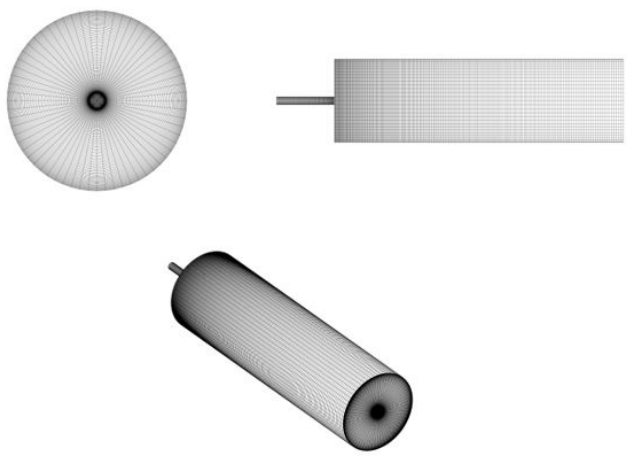

Figure 4.2: Mesh resolution used in this study.

A pressure-based solver is used to solve the compressible Navier-Stokes equation. Filtered continuity, momentum, energy, and species equation for the mass fraction of helium are solved, and the Dynamic Smagorinsky model is used to account for the subgrid scales effect.

The precursor simulation is performed in a pipe with streamwise periodic boundary conditions, using the SST k-ω model. No-slip and adiabatic boundary conditions are applied at the inner and outer pipe walls, and outflow boundary conditions are applied at the domain's downstream end. Uniform velocity profiles without perturbations are used at the air inlet, and fully developed profiles of x-velocity, turbulent kinetic energy, and turbulent dissipation rate, obtained from a precursor RANS simulation and perturbed by the Vortex Method, are applied at the helium inlet, in which 190 vortices are generated. At both inlets, uniform temperature profiles of $T = 300K$ are used.

The numerical methods used are Fractional Step Method to handle the pressure-velocity coupling, Least Squares to compute gradients, Central Differencing scheme to interpolate

convective terms of momentum, energy, and species equation and also to interpolate pressure and Bounded Second-Order Implicit to march solution in time, with a fixed time step of Δt=0.00369D/U_j, ensuring CFL≈0.1.

To quickly reach the statistically steady-state, a disturbed velocity field and a species field, both obtained from a converged RANS simulation, are used to initialize the solution. The RANS simulation is calculated using the SST k-ω model.

4.3.3 LES: Verification and Validation

The grid sensitivity analysis is conducted for the LES simulation performed in a commercially available software. The computational grid sensitivity analysis is accomplished by using three different sets of grids, each containing 4 million, 8 million, and 16 million cells, respectively. The mean axial velocity profiles along the centerline do not vary for the last two grid sizes used, hence conforming to a grid-independent solution. Thus, a grid size of 8 million cells is used in this analysis.

4.4 Echo State Network

An input vector $u(t)$ with K units are fed into a dynamic 'Reservoir' with N units in a generic Echo State Network (ESN). The reservoir is connected to an output layer $y(t)$ with N_y units. At discrete time t, the reservoir receives input, subsequently coupled with the reservoir state to produce output at $t + \delta t$.

In Echo State Networks, an RNN with leaky-integrated discrete-time continuous-value units is employed. The following are the ESN equations:

$$\widetilde{x(n)} = \tanh(W^{in}[1; u(n)] + Wx(n-1)) \tag{4.5}$$

$$x(n) = (1-\alpha)x(n-1) + \alpha\widetilde{x}(n) \tag{4.6}$$

where $x(n)$ is the activation of reservoir neurons and $\widetilde{x(n)}$ is the update at each time step n. One of the most popular choices is the sigmoid wrapper $tanh()$. W^{in} and W are the in-

put weight matrix and recurrent weight matrix, respectively, $\alpha \in (0,1]$ is the leaking rate, [;] represents a vertical vector (or matrix) concatenation [61]. After the reservoir has been trained, the output weight matrix is created using linear regression. The following is the definition of the linear readout layer:

$$y(n) = W^{out}[1; u(n); x(n)] \tag{4.7}$$

4.4.1 Pseudo-Algorithm

According to Jaeger [47], the original Echo State Network approach is as follows:

- Using the input weight matrix W^{in}, the recurrent weight matrix W, and the leaking rate α, a random reservoir is created.
- The network is run using the training inputs u(n), and reservoir activation units x(n) are collected.
- The network output is calculated using the linear readout layer. The W^{out} output weights are computed. This is done by reducing the mean-squared error between the predicted output and the target output.
- Now that the network is trained, the output is calculated on the unseen data.

4.4.2 ESN-Training

The purpose of ESN training, is to learn the weights of the output matrix by mapping a set of inputs $u(t)$ to a higher dimensional reservoir over a discrete-time period $-T \leq t \leq 0$. This is accomplished by reducing the least square error between the network's output $y(n)$ and the target output $y^{target}(n)$ as illustrated in equation 4.8. The random generation of the weight input matrix W^{in} and the recurrent weight matrix W makes the output weight matrix calculation a linear regression problem. Several hyperparameters are tuned to get a set of optimum output weights.

$$E(y, y^{t\arg et}) = \frac{1}{N}\sum_{i=1}^{N}\sqrt{\frac{1}{T}\sum_{n=1}^{T}\left(y_i(n) - {y_i}^{t\arg et}(n)\right)^2} \tag{4.8}$$

4.4.3 ESN-Testing

The inputs are replaced with the network's predicted output $y(t)$, which is used as a driving signal to the reservoir for $t \geq 0$, which results in an autonomous system prediction. The mean squared error (MSE) is a statistic used to assess ESN's performance on the test data.

The Echo State Property of the ESN reservoir precludes a longer-term prediction of turbulent jet behavior at this time. This is owing to the fact that the amplitude of the driving signal to the reservoir will decrease with time. Longer-term prediction of chaotic behavior is impossible, according to Lorenz [58] work. Longer-term flow predictions are difficult because turbulent flows are fundamentally chaotic. As a result, the Echo State Property does not always decrease the ESN method's effectiveness.

4.4.4 ESN: Parallel Implementation

The reservoir size restriction is another weakness in the ESN method. As the number of nodes in the reservoir increases, the computational cost of tuning the hyperparameters rises, lengthening the time it takes to build a functional model that accurately predicts flow field behavior. This was not a problem for the overwhelming majority of the predictions made throughout this study. The Q-criterion became prohibitive due to the large number of neurons needed to predict the turbulent vorticity field. To address this problem, ESN was utilized in parallel mode.

For the ESN model to run in parallel, the flow field was split into several spatial regions. A different ESN reservoir predicts each domain. The locality parameter is utilized in the flow field to establish continuity between two nearby spatial regions. Each reservoir develops in parallel during training, resulting in a unique set of output weights. This method was successfully used by Pathak et al. [74] to predict the dynamics of the Kuramato-Shivansky equation.

4.5 Results

The results of the current investigation are listed below. Statistically averaging of the data predicted by the Echo State Network over time yields the mean flow properties. Parallel architecture of the reservoir is employed to obtain the whole turbulent field. The instantaneous vortical structures predicted by ESN for the Helium jet are plotted and compared to LES.

4.5.1 ESN Hyperparameters

Some of the hyperparameters are listed in table 4.2. A comprehensive grid search was performed to obtain a set of hyperparameters for each type of jet.

Table 4.2: Hyper parameters used for different jets

Hyperparameters	He	Air	CO_2
Leak rate	0.2	0.1	0.1
Size of the reservoir	1000	1000	800
Regularization coefficient	1e-07	1e-07	1e-08
Probability of non-zero connections	0.22	0.1	0.1
No of groups	200	-	-
Locality parameter	2000	-	-

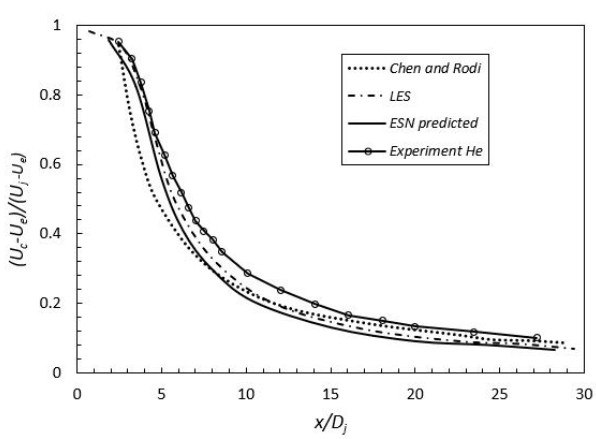

Figure 4.3: Mean axial velocity profile for Helium

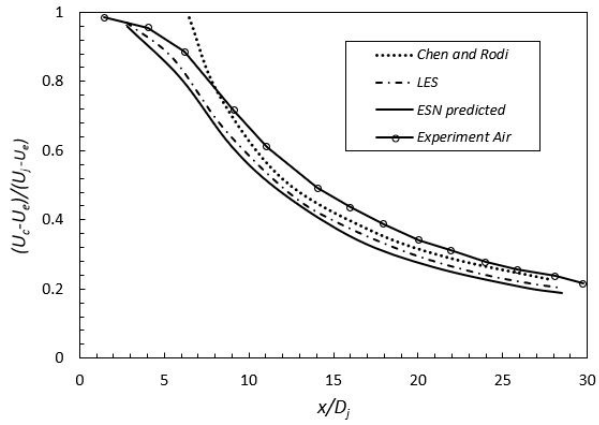

Figure 4.4: Mean axial velocity profile for air

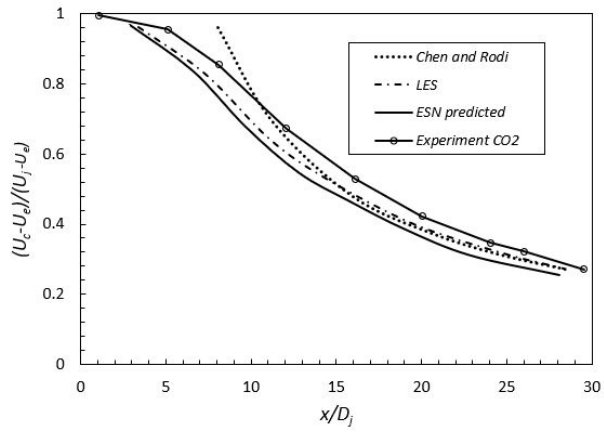

Figure 4.5: Mean axial velocity profile for carbon-dioxide

4.5.2 Comparison of mean flow properties

The profiles of mean axial velocity, rms fluctuations along the jet axis, radial profiles of the mean axial velocity, and shear stresses are shown. The results obtained from ESN are compared with the experiment for all three jets. The detailed discussions of results are presented.

Axial velocity profiles

Figures 4.3, 4.4 and 4.5 show a detailed comparison of the mean velocity profiles for the three jets, obtained from ESN to the experiment and similarity laws obtained by Chen and Rodi [24]. In comparison to heavier gases, the helium jet's centerline velocity decayed

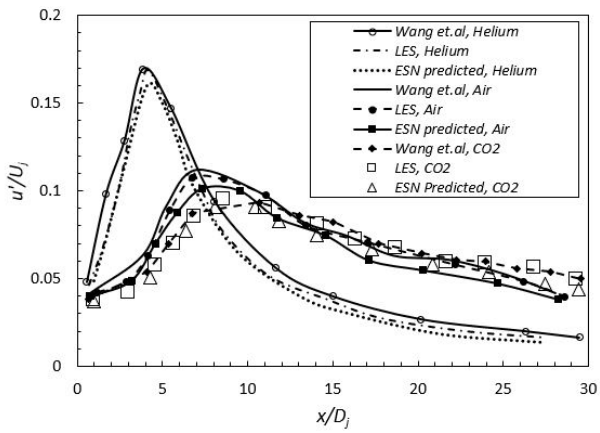

Figure 4.6: Axial rms velocity fluctuations for the three jets

much faster. The ESN captured the impact of density variation well, and the results are in good agreement with the experiment. The profiles of heavier jets appeared to alter, which could be owing to minor variances in inflow conditions.

The impact of density difference on the centerline velocity is also described by the similarity laws proposed by Chen and Rodi [24]. ESN demonstrated excellent agreement for Helium jets, while profiles for heavier jets appeared to differ. This could be explained by the approximate nature of the similarity laws.

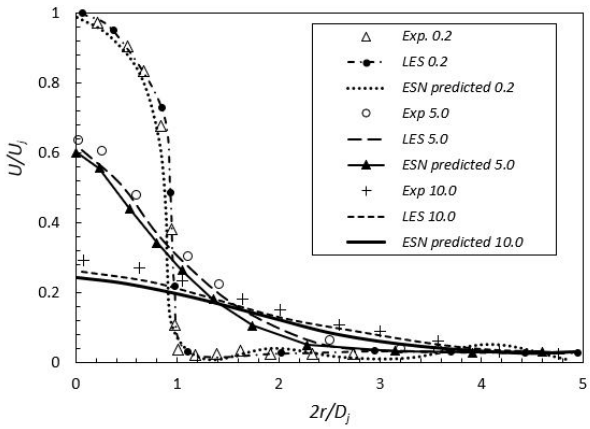

Figure 4.7: Normalised radial streamwise velocity at various axial locations, Helium jet

Axial rms profiles

Figure 4.6 shows the axial velocity fluctuations for all three jets predicted by ESN, and the plots are compared with the current LES and LES simulation performed by Wang et al. [96]. As can be seen, the rms fluctuations predicted by ESN are in very good agreement with the simulations performed by Wang et al. [96]. The lighter Helium jet decayed much faster than, the heavier jets, as it mixes with the ambient air much faster, leading to an increase in turbulence intensity. The peak rms value for Helium is obtained much earlier, and the magnitude is much higher compared with heavier jets. The Kelvin-Helmholtz instability grows, causing the rms values near the potential core to rise faster over the shear layer.

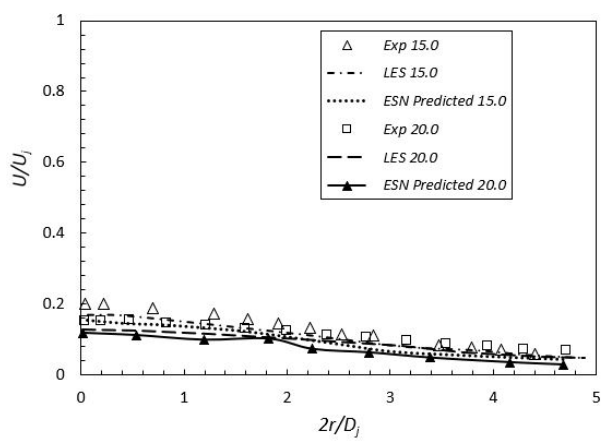

Figure 4.8: Normalised radial streamwise velocity at various axial locations, Helium jet

Radial profiles of mean streamwise velocity

Figures 4.7 and 4.8 illustrate radial profiles of mean normalised streamwise velocity (U/U_j) for the Helium jet at various axial locations (x/D_j). The ESN predictions obtained demonstrated a high level of agreement with the experiment. After comparing the present LES findings to the experiment and the validated LES results, ESN training and testing were obtained.

The radial profiles of centerline velocity decrease for various axial locations(x/D_j), starting

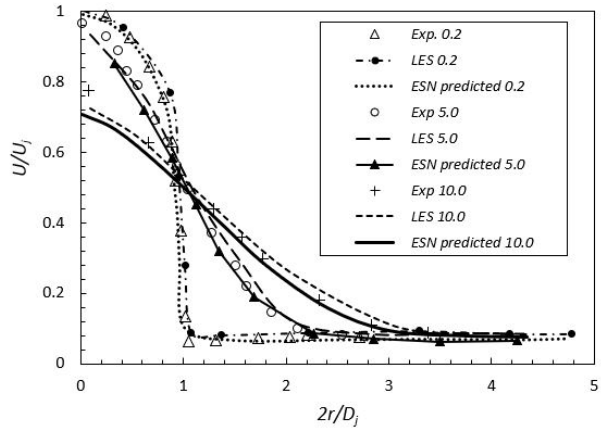

Figure 4.9: Normalised radial streamwise velocity at various axial locations, CO_2 jet

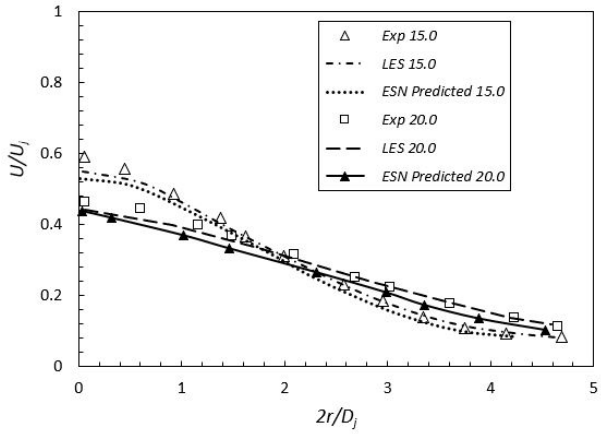

Figure 4.10: Normalised radial streamwise velocity at various axial locations, CO_2 jet

from x/D_j)=0.2 to x/D_j=20. At x/D_j=0.2, the profile is similar to a turbulent pipe flow and has the highest initial velocity.

Similarly, the profiles for CO_2 are shown in figures 4.9 and 4.10. The profiles for the air jet are similar to that of CO_2 jet. There was some difference between the experiment and LES results, which could be due to the flow not being fully developed at x/D_j=0.2, but otherwise, the experiment and LES results were in good agreement. Although there is a small variation between the results predicted by ESN and the actual results, ESN predicted the trend adequately. The decaying nature of mean streamwise velocity is also captured by ESN.

Radial profiles of rms fluctuations at various axial locations

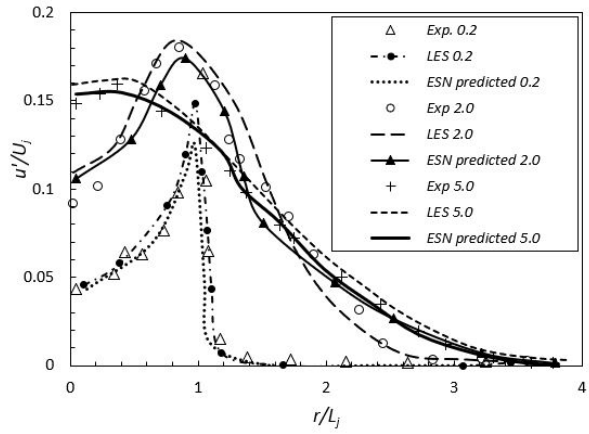

Figure 4.11: rms fluctuations of streamwise velocity at various axial locations, He jet

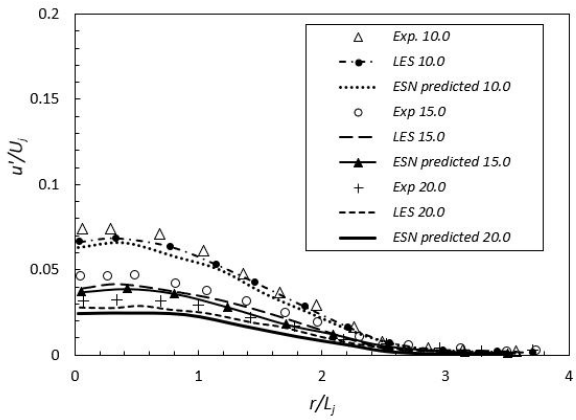

Figure 4.12: rms fluctuations of streamwise velocity at various axial locations, He jet

The radial profiles of rms streamwise velocity fluctuations along various axial locations are shown in figures 4.11, 4.12, 4.13 and 4.14. The radial co-ordinates were normalised by the local velocity half width L_j, where L_j is defined as the distance where the difference of velocity at any point and co-flow velocity is equal to the difference between the centerline velocity and the co-flow velocity , i.e. $U - U_e = 0.5(U_c - U_e)$. Similar approach was used in Wang et al. [96] and the experiments by Amielh et al. [2].

For x/D_j=0.2, a peak value of 0.15 was attained by both jets at the shear layer, whereas at the axis, a value of 0.04 was reached. As we moved further downstream, rms values

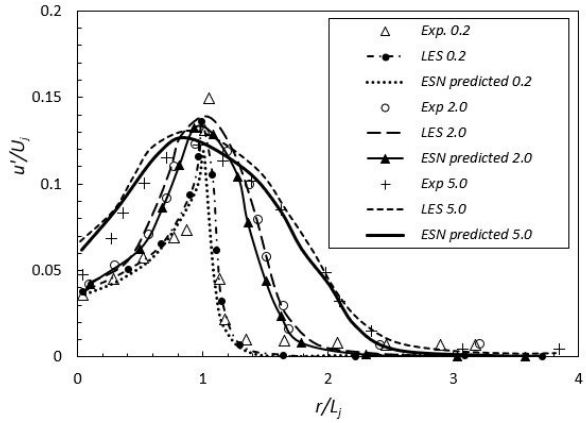

Figure 4.13: rms fluctuations of streamwise velocity at various axial locations, CO_2 jet

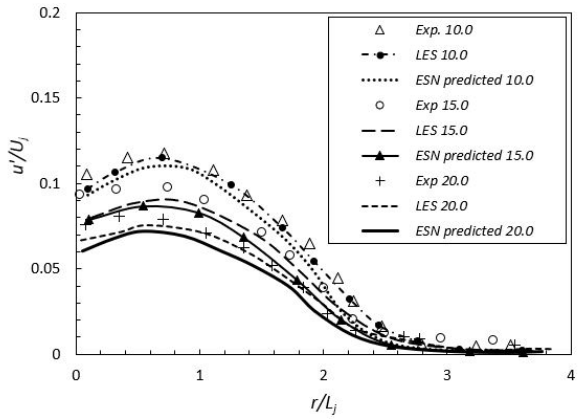

Figure 4.14: rms fluctuations of streamwise velocity at various axial locations, CO_2 jet

along the axis increased as a result of growth in jet mixing. Further downstream, the profiles reached a state of self-similarity. ESN was shown to predict this behavior well. This transition was much faster in the Helium jet compared to the CO_2 jet.

Radial profiles of shear stress

Radial profiles of shear stress distribution for Helium and CO_2 jet normalised by the jet half-width are shown in figures 4.15, 4.16, 4.17 and 4.18. For clarity, the vertical axes of the two jets are scaled differently. The shear stress profiles predicted by the ESN for the Helium jet showed an excellent agreement with the experiment and LES performed by Wang et al. [96] compared to the CO_2 jet.

The peak value predicted at the x/D_j=0.2 was only 0.003 for the Helium jet. The ESN

slightly under-predicted this value. It is difficult to capture the exact value at this region as the flow was not fully developed yet. As the flow moved towards the downstream region (x/D_j=2.0), the profile became smoother, and the magnitude of shear stress was almost four times the initial value. Further downstream, the shear stress decayed as the jet broadened and the gradient values decreased.

For the CO_2 jet, the peak value at the jet outlet was higher than the Helium jet. As the flow was not fully developed, it is difficult to capture this peak. The values predicted by LES and ESN at x/D_j=2.0 and x/D_j=5.0 were higher than the experiment values but had the correct profile shapes. Further downstream, the agreement between the experiment results and the ESN results was good. The differences in the shapes were due to the higher Reynolds number in the case of CO_2 jet than the Helium jet. The mean turbulent viscosity observed near the shear layer was close to 2.4 μ in the CO_2 jet, while 0.5 μ for the Helium jet.

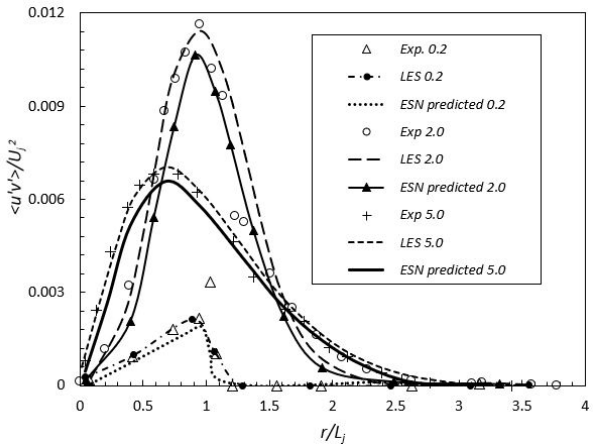

Figure 4.15: radial shear stress profiles at various axial locations, He jet

4.5.3 Coherent structures

Figures 4.19 and 4.20 show the Q-criterion of isosurface for helium jet predicted from the LES simulation and ESN prediction, respectively. The Q-criterion plot allows the investigation of the development of the coherent structures responsible for momentum and mass exchange on a large scale. The value of Q was adjusted for an optimal representation of

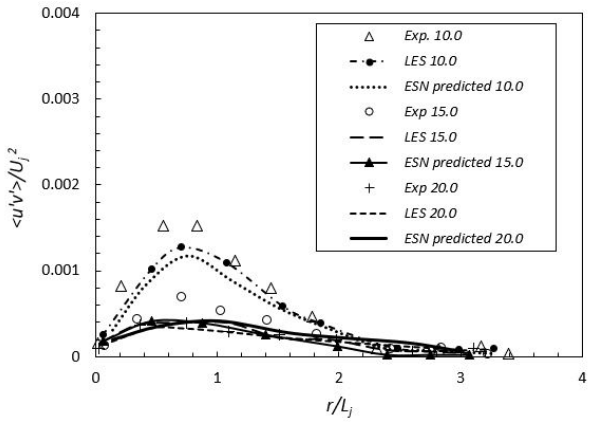

Figure 4.16: radial shear stress profiles at various axial locations, He jet

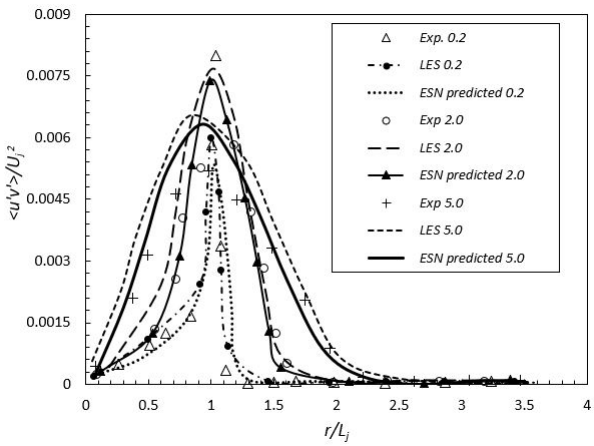

Figure 4.17: radial shear stress profiles at various axial locations, CO_2 jet

the vortical structures. In the immediate region of the jet, vortex rings formed due to the Kelvin-Helmholtz instability. Further downstream, the shear layer became unstable, resulting in large-scale vortices formed due to vortex coupling. For the Helium jet, near the nozzle, the distance between the vortex rings was higher, and the size of the vortex rings was larger. This is observed up to an axial length of x/D_j=18, after which the large-scale turbulent structures were more homogeneous and could not be distinguished.

The parallel implementation of ESN was used to predict the vortical structures formed. ESN captured the vortex rings formed near the jet exit, and as the jet moved further downstream, ESN predicted the formation of large scale turbulent structures. The prediction of vortical structures demonstrates ESN's capability to capture turbulent behavior of variable-

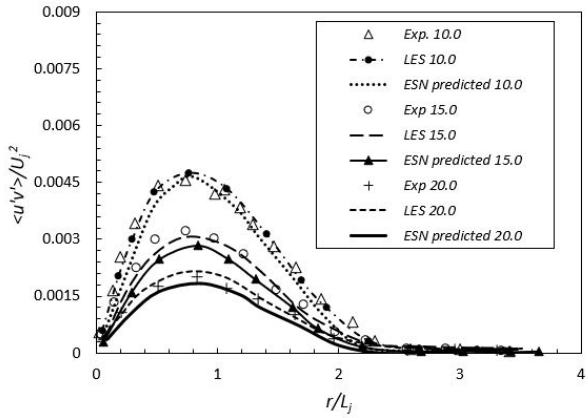

Figure 4.18: radial shear stress profiles at various axial locations, CO_2 jet

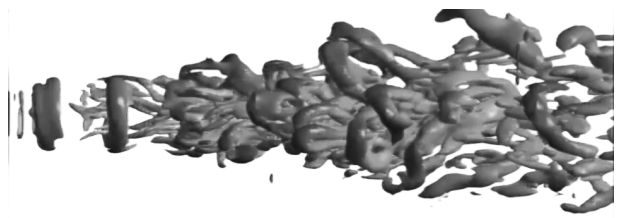

Figure 4.19: Vortical structures obtained from LES simulation for He jet. Shown here are the isosurface of Q criterion at a Q value of 50000

density turbulent jets.

4.6 Conclusion

The flow behavior of variable-density jets has been effectively captured using an ESN model. The following observations were made based on the results of this study:

- ESN captured the decaying nature of mean centerline velocity, and the agreement with the experiment was good. In comparison to heavier jets, the velocity of lighter Helium jets diminished much faster.

- The turbulent intensities predicted by the ESN were in excellent agreement with the previously published simulation results. The lighter Helium jet decayed much faster than, the heavier jets, consistent with previous studies. The peak value predicted by the ESN was much higher in magnitude for the Helium jet compared to the heavier air and CO_2.

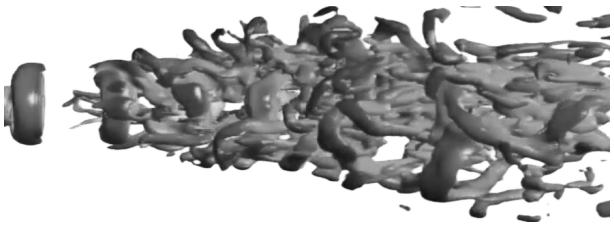

Figure 4.20: Vortical structures obtained from ESN modeling for He jet. Shown here are the isosurface of Q criterion at a Q value of 50000

- The radial profiles of mean streamwise velocity and rms fluctuations along several axial locations were predicted by ESN and demonstrated a high level of agreement with the experiment.

- The parallel architecture of ESN proved successful in capturing the vortical structures of the Helium jet. The ESN results demonstrated an excellent qualitative agreement with the LES results. The parallel architecture of ESN improved its ability to handle large-scale data sets.

- The radial profiles of shear stress were evaluated using an ESN model. The ESN model predicted the correct profile shapes of shear stress for Helium and CO_2 jets.

- One of the significant limitations of the ESN was, it could only be used for short-term prediction. Over time, the driving signal to the reservoir vanished, limiting the ESN's long-term predictive capability.

In conclusion, an ESN can successfully replicate variable-density jet flow field behavior, and it represents a promising research area that warrants additional investigation.

CHAPTER 5

CONCLUSIONS

In the present study, an ESN model has been successfully used to model turbulent jet flow behavior. This is the first time an approach like this has been used. ESN provided a model-free estimation of turbulent jet flow behavior, which is the biggest takeaway from this research.

For the first investigation, an Echo State Network (ESN) has been successfully used to model the short-term dynamic behavior of a turbulent free jet issuing into a quiescent medium. This is the first time ESNs have been used to model such a flow field. Based on the results obtained during the course of this study, the following conclusions may be drawn:

- The ESN model quantitatively modeled the mean axial centerline velocity for all Reynolds numbers considered, with a maximum difference between ESN and LES testing results being on the order of 0.02. The ESN was also able to predict the decaying nature of the mean axial centerline velocity.

- The ESN model quantitatively modeled the rms axial velocity fluctuations for all Reynolds numbers considered. The ESN results also displayed the previously observed functional dependence on Reynolds number of the rms velocity fluctuations.

- A parallelized version of the ESN model qualitatively captured the vortical structure of the jet for a Reynolds number of 3600. Parallelizing the ESN expanded the ability of the model to handle the larger-scale datasets associated with the instantaneous, three-dimensional vorticity field.

- The ESN model modeled the shear layer frequencies for all Reynolds numbers considered. The ESN model was also able to predict the peak frequency of the energy spectra associated with the axial velocity fluctuations. The ESN model modeled a peak frequency value of 0.016 compared to a value of 0.017 obtained from inviscid instability theory.

- The ESN model modeled that the jet-preferred mode would be dependent on the Reynold number and the momentum thickness. This agreed well with previously published experimental results for Strouhal numbers in the range of 0.3 to 0.6.

- The ESN model modeled that the asymmetric mode [mode 0] was dominant at the jet exit, but past the potential core the double-helix mode [mode 2] became dominant. This was consistent with previously published LES results.

- A limitation of the ESN modeling approach was that as prediction times increased, the Echo State Property of the ESN reservoir resulted in a vanishing driving signal. This loss of signal limits the long-term predictive capability of ESN.

For the second investigation, an ESN has been used to model a hot jet issuing from a nozzle into cold air in the opposite direction of gravity. The following conclusions were drawn based on the study:

- The ESN model modeled the decaying nature of mean centerline velocity and mean centerline temperature. The maximum difference observed between the decay laws and ESN's results were on the order of 0.03. The ESN model also captured the self-similarity behavior of the mean axial velocity distribution along the radial direction.

- The ESN model correctly modeled the axial velocity and temperature fluctuations along the jet. The ESN model also correctly calculated the peak values of turbulent intensities for both cases considered in this study. The ESN was used to measure

the radial velocity fluctuations along different streamwise locations for Case 2 and demonstrated an excellent agreement with the experiment fit data.

- The parallel architecture of the ESN was used to capture the vortical evolution of the jet at a Reynolds number of 8000, and a good qualitative agreement with the simulation was obtained. The capacity of the model to handle larger-scale datasets related with the instantaneous, three-dimensional vorticity field was improved by parallelizing the ESN.

- The ESN model correctly modeled the decreasing nature of mean turbulent kinetic energy with increasing temperature gradient value. This was consistent with previously published LES results.

- One of the limitations of the ESN model was its inability to predict long data sequences. The driving signal to the reservoir vanishes over time which limits the predictive capability of ESN.

Finally, for the third investigation, the flow behavior of variable-density jets has been effectively captured using an ESN model. The following observations were made based on the results of this study:

- ESN captured the decaying nature of mean centerline velocity, and the agreement with the experiment was good. In comparison to heavier jets, the velocity of lighter Helium jets diminished much faster.

- The turbulent intensities modeled by the ESN were in excellent agreement with the previously published simulation results. The lighter Helium jet decayed much faster than, the heavier jets, consistent with previous studies. The peak value modeled by the ESN was much higher in magnitude for the Helium jet compared to the heavier air and CO_2.

- The radial profiles of mean streamwise velocity and rms fluctuations along several axial locations were modeled by ESN and demonstrated a high level of agreement with the experiment.

- The parallel architecture of ESN proved successful in capturing the vortical structures of the Helium jet. The ESN results demonstrated an excellent qualitative agreement with the LES results. The parallel architecture of ESN improved its ability to handle large-scale data sets.

- The radial profiles of shear stress were evaluated using an ESN model. The ESN model modeled the correct profile shapes of shear stress for Helium and CO_2 jets.

- One of the significant limitations of the ESN was, it could only be used for short-term prediction. Over time, the driving signal to the reservoir vanished, limiting the ESN's long-term predictive capability.

The present work successfully depicts the modeling capability of an ESN for turbulent jet flows. For all the cases considered, the ESN model successfully replicated the flow behavior with some discrepancies from the LES results. As the Reynolds numbers increased, the discrepancy between the LES and ESN results was high. This could be attributed to hyperparameters, precisely the size of the reservoir. The size of the reservoir can be further tuned to achieve greater accuracy in modeling turbulent jet behavior for higher Reynolds number values.

For future works, transfer learning could be implemented with an ESN model. The output weights generated for a particular case of Reynolds number can be further used for other Reynolds numbers. The goal of transfer learning would be to avoid training a different ESN model for each flow case. The hyperparameters in the new cases can be further tuned to achieve better accuracy in modeling similar flows. With some modifications to the hyperparameters, transfer learning will save a considerable amount of computational time required to train an ESN model.

One of the significant limitations of an ESN is that it can only be used for short-term predictions of spatio-temporal dynamic systems. To overcome this, an ESN can be combined with other RNNs like LSTMs to improve its long-term predictive capability. Because there may be delays of undetermined length between significant occurrences in a time series, LSTM networks are well-suited to classifying, processing, and generating predictions based on time series data. LSTMs were created to solve the issue of vanishing gradients that may occur while training conventional RNNs. If feedbacks are added to an ESN model, it has the potential of enhancing its predictive capability, which warrants future investigation.

REFERENCES

[1] SA Ahmed, RMC So, and HC Mongia. Density effects on jet characteristics in confined swirling flow. *Experiments in fluids*, 3(4):231–238, 1985.

[2] M Amielh, T Djeridane, F Anselmet, and L Fulachier. Velocity near-field of variable density turbulent jets. *International Journal of Heat and mass transfer*, 39(10):2149–2164, 1996.

[3] Susan M Anderson and Klaus Bremhorst. Investigation of the flow field of a highly heated jet of air. *International journal of heat and fluid flow*, 23(2):205–219, 2002.

[4] RA Antonia, LWB Browne, AJ Chambers, and S Rajagopalan. Budget of the temperature variance in a turbulent plane jet. *International Journal of Heat and Mass Transfer*, 26(1):41–48, 1983.

[5] Piotr Antonik, Anteo Smerieri, François Duport, Marc Haelterman, and Serge Massar. Fpga implementation of reservoir computing with online learning. In *24th Belgian-Dutch Conference on Machine Learning*, 2015.

[6] David Babcock, Changhoon Lee, Bhusan Gupta, John Kim, and Rodney Goodman. Active drag reduction using neural networks. In *Proceedings of International Workshop on Neural Networks for Identification, Control, Robotics and Signal/Image Processing*, pages 279–287. IEEE, 1996.

[7] Jawaid Bashir and Mahinder S Uberoi. Experiments on turbulent structure and heat transfer in a two-dimensional jet. *The Physics of Fluids*, 18(4):405–410, 1975.

[8] GK Batchelor and A Eo Gill. Analysis of the stability of axisymmetric jets. *Journal of Fluid Mechanics*, 14(4):529–551, 1962.

[9] Christopher M Bishop. *Pattern recognition and machine learning*. springer, 2006.

[10] Daniel J Bodony and Sanjiva K Lele. On using large-eddy simulation for the prediction of noise from cold and heated turbulent jets. *Physics of Fluids*, 17(8):085103, 2005.

[11] Christophe Bogey and Christophe Bailly. Effects of inflow conditions and forcing on subsonic jet flows and noise. *AIAA journal*, 43(5):1000–1007, 2005.

[12] Sami Boujemaa, Muriel Amielh, and Marie Pierre Chauve. Velocity and concentration distributions in globally unstable axisymmetric helium jets. *Comptes Rendus Mécanique*, 335(8):449–454, 2007.

[13] P Bradshaw. The effect of initial conditions on the development of a free shear layer. *Journal of Fluid Mechanics*, 26(2):225–236, 1966.

[14] LWB Browne, RA Antonia, and AJ Chambers. The interaction region of a turbulent plane jet. *Journal of fluid mechanics*, 149:355–373, 1984.

[15] Thomas L Carroll. Mutual information and the edge of chaos in reservoir computers. *arXiv preprint arXiv:1906.03186*, 2019.

[16] Thomas L Carroll. Dimension of reservoir computers. *Chaos: An Interdisciplinary Journal of Nonlinear Science*, 30(1):013102, 2020.

[17] TL Carroll. Path length statistics in reservoir computers. *Chaos: An Interdisciplinary Journal of Nonlinear Science*, 30(8):083130, 2020.

[18] Rohitash Chandra and Mengjie Zhang. Cooperative coevolution of elman recurrent neural networks for chaotic time series prediction. *Neurocomputing*, 86:116–123, 2012.

[19] Sarah Chang and Daniel Lathrop. Using reservoir computing to predict temperature fluctuations in turbulent rayleigh-bénard convection. In *APS Division of Fluid Dynamics Meeting Abstracts*, pages NP05–008, 2019.

[20] Bruno Chaouat. The state of the art of hybrid rans/les modeling for the simulation of turbulent flows. *Flow, turbulence and combustion*, 99(2):279–327, 2017.

[21] Patrick Chassaing, RA Antonia, Fabien Anselmet, L Joly, and Sahotra Sarkar. *Variable density fluid turbulence*, volume 69. Springer Science & Business Media, 2002.

[22] Sotirios P Chatzis and Yiannis Demiris. Echo state gaussian process. *IEEE Transactions on Neural Networks*, 22(9):1435–1445, 2011.

[23] Sotirios P Chatzis and Yiannis Demiris. The copula echo state network. *Pattern Recognition*, 45(1):570–577, 2012.

[24] Ching Jen Chen and Wolfgang Rodi. Vertical turbulent buoyant jets: a review of experimental data. *STIA*, 80:23073, 1980.

[25] Emanuela Colombo, Fabio Inzoli, Adriano Muzzio, and J Teatini. Les modelling for free, incompressible and non-isothermal round jet. In *5th European Thermal-Sciences Conference*, pages 1–8, 2008.

[26] T Colonius and J Freund. Pod analysis of sound generation by a turbulent jet. In *40th AIAA Aerospace Sciences Meeting & Exhibit*, page 72, 2002.

[27] DG Crighton and M Gaster. Stability of slowly diverging jet flow. *Journal of Fluid Mechanics*, 77(2):397–413, 1976.

[28] AE Davies, JF Keffer, and WD Baines. Spread of a heated plane turbulent jet. *The physics of fluids*, 18(7):770–775, 1975.

[29] Niels G Deen, EAJF Peters, Johan T Padding, and JAM Kuipers. Review of direct numerical simulation of fluid–particle mass, momentum and heat transfer in dense gas–solid flows. *Chemical Engineering Science*, 116:710–724, 2014.

[30] Eugen Diaconescu. The use of narx neural networks to predict chaotic time series. *Wseas Transactions on computer research*, 3(3):182–191, 2008.

[31] T Djeridane, M Amielh, F Anselmet, and L Fulachier. Velocity turbulence properties in the near-field region of axisymmetric variable density jets. *Physics of Fluids*, 8(6):1614–1630, 1996.

[32] Peter F Dominey. Complex sensory-motor sequence learning based on recurrent state representation and reinforcement learning. *Biological cybernetics*, 73(3):265–274, 1995.

[33] Paul A Durbin. A perspective on recent developments in rans modeling. In *Engineering Turbulence Modelling and Experiments 5*, pages 3–16. Elsevier, 2002.

[34] Aida A Ferreira, Teresa B Ludermir, and Ronaldo RB De Aquino. An approach to reservoir computing design and training. *Expert systems with applications*, 40(10):4172–4182, 2013.

[35] Holger Foysi, Juan P Mellado, and Sutanu Sarkar. Large-eddy simulation of variable-density round and plane jets. *International Journal of Heat and Fluid Flow*, 31(3):307–314, 2010.

[36] Masataka Gamahara and Yuji Hattori. Searching for turbulence models by artificial neural network. *Physical Review Fluids*, 2(5):054604, 2017.

[37] Peter John Gehrke. *The Turbulent Kinetic Energy Balance of a Fully Pulsed Axisymmetric Jet: Processing and Analysis Programs (Appendix 6)*. PhD thesis, University of Queensland, 1996.

[38] Massimo Germano, Ugo Piomelli, Parviz Moin, and William H Cabot. A dynamic subgrid-scale eddy viscosity model. *Physics of Fluids A: Fluid Dynamics*, 3(7):1760–1765, 1991.

[39] Felix Grezes. *Reservoir Computing*. PhD thesis, PhD thesis, The City University of New York, 2014.

[40] Ephraim Gutmark and Chih-Ming Ho. Preferred modes and the spreading rates of jets. *The Physics of fluids*, 26(10):2932–2938, 1983.

[41] MP Hallberg and PJ Strykowski. On the universality of global modes in low-density axisymmetric jets. *Journal of Fluid Mechanics*, 569:493, 2006.

[42] Min Han, Jianhui Xi, Shiguo Xu, and Fu-Liang Yin. Prediction of chaotic time series based on the recurrent predictor neural network. *IEEE transactions on signal processing*, 52(12):3409–3416, 2004.

[43] K Hanjalic. Will rans survive les? a view of perspectives. 2005.

[44] C-M Ho and Patrick Huerre. Perturbed free shear layers. *AnRFM*, 16:365–424, 1984.

[45] AKMF Hussain and MF Zedan. Effects of the initial condition on the axisymmetric free shear layer: Effect of the initial fluctuation level. *The Physics of Fluids*, 21(9):1475–1481, 1978.

[46] Matthias Ihme, Christoph Schmitt, and Heinz Pitsch. Optimal artificial neural networks and tabulation methods for chemistry representation in les of a bluff-body swirl-stabilized flame. *Proceedings of the Combustion Institute*, 32(1):1527–1535, 2009.

[47] Herbert Jaeger. The "echo state" approach to analysing and training recurrent neural networks-with an erratum note. *Bonn, Germany: German National Research Center for Information Technology GMD Technical Report*, 148(34):13, 2001.

[48] PE Jenkins and VW Goldschmidt. Mean temperature and velocity in a plane turbulent jet. 1973.

[49] R Jester-Zürker, S Jakirlić, and C Tropea. Computational modelling of turbulent mixing in confined swirling environment under constant and variable density conditions. *Flow, turbulence and combustion*, 75(1-4):217–244, 2005.

[50] Daehan Jung, Stephan Gamard, and William K George. Downstream evolution of the most energetic modes in a turbulent axisymmetric jet at high reynolds number. part 1. the near-field region. *Journal of Fluid Mechanics*, 514:173–204, 2004.

[51] Soteris A Kalogirou. Artificial intelligence for the modeling and control of combustion processes: a review. *Progress in energy and combustion science*, 29(6):515–566, 2003.

[52] Jungwoo Kim and Haecheon Choi. Large eddy simulation of a circular jet: effect of inflow conditions on the near field. *Journal of Fluid Mechanics*, 620:383, 2009.

[53] Sanjukta Krishnagopal, Michelle Girvan, Edward Ott, and Brian R Hunt. Separation of chaotic signals by reservoir computing. *Chaos: An Interdisciplinary Journal of Nonlinear Science*, 30(2):023123, 2020.

[54] DM Kyle and KR Sreenivasan. The instability and breakdown of a round variable-density jet. *Journal of Fluid Mechanics*, 249:619–664, 1993.

[55] C Le Ribault, S Sarkar, and SA Stanley. Large eddy simulation of a plane jet. *Physics of fluids*, 11(10):3069–3083, 1999.

[56] Lutz Lesshafft, Patrick Huerre, Pierre Sagaut, and Marc Terracol. Nonlinear global modes in hot jets. 2006.

[57] Xiaowei Lin, Zehong Yang, and Yixu Song. Short-term stock price prediction based on echo state networks. *Expert systems with applications*, 36(3):7313–7317, 2009.

[58] Edward N Lorenz. Deterministic nonperiodic flow. *Journal of atmospheric sciences*, 20(2):130–141, 1963.

[59] Zhixin Lu, Brian R Hunt, and Edward Ott. Attractor reconstruction by machine learning. *Chaos: An Interdisciplinary Journal of Nonlinear Science*, 28(6):061104, 2018.

[60] Zhixin Lu, Jaideep Pathak, Brian Hunt, Michelle Girvan, Roger Brockett, and Edward Ott. Reservoir observers: Model-free inference of unmeasured variables in chaotic systems. *Chaos: An Interdisciplinary Journal of Nonlinear Science*, 27(4):041102, 2017.

[61] Mantas Lukoševičius. A practical guide to applying echo state networks. In *Neural networks: Tricks of the trade*, pages 659–686. Springer, 2012.

[62] Wolfgang Maass, Thomas Natschläger, and Henry Markram. Real-time computing without stable states: A new framework for neural computation based on perturbations. *Neural computation*, 14(11):2531–2560, 2002.

[63] Michael C Mackey and Leon Glass. Oscillation and chaos in physiological control systems. *Science*, 197(4300):287–289, 1977.

[64] J Mi, D Nobes, and G Nathan. Influence of jet exit conditions on the passive scaler field of an axisymmetric free jet. 2001.

[65] Alfons Michalke. On the inviscid instability of the hyperbolictangent velocity profile.

Journal of Fluid Mechanics, 19(4):543–556, 1964.

[66] Arvind T Mohan, Dima Tretiak, Misha Chertkov, and Daniel Livescu. Spatio-temporal deep learning models of 3d turbulence with physics informed diagnostics. *Journal of Turbulence*, 21(9-10):484–524, 2020.

[67] Parviz Moin and Krishnan Mahesh. Direct numerical simulation: a tool in turbulence research. *Annual review of fluid mechanics*, 30(1):539–578, 1998.

[68] PA Monkewitz. The role of absolute and convective instability in predicting the behavior of fluid systems. *EJMF*, 9(5):395–413, 1990.

[69] Peter A Monkewitz, Bernhard Lehmann, Bernd Barsikow, and Dietrich W Bechert. The spreading of self-excited hot jets by side jets. *Physics of Fluids A: Fluid Dynamics*, 1(3):446–448, 1989.

[70] Peter A Monkewitz and Eberhard Pfizenmaier. Mixing by side jets"in strongly forced and self-excited round jets. *Physics of Fluids A: Fluid Dynamics*, 3(5):1356–1361, 1991.

[71] Joseph W Nichols, Peter Schmid, and James J Riley. Self-sustained oscillations in variable-density round jets. 2007.

[72] Nagangudy R Panchapakesan and John L Lumley. Turbulence measurements in axisymmetric jets of air and helium. part 1. air jet. *Journal of Fluid Mechanics*, 246:197–223, 1993.

[73] Sandeep Pandey and Jörg Schumacher. Reservoir computing model of two-dimensional turbulent convection. *Physical Review Fluids*, 5(11):113506, 2020.

[74] Jaideep Pathak, Brian Hunt, Michelle Girvan, Zhixin Lu, and Edward Ott. Model-free prediction of large spatiotemporally chaotic systems from data: A reservoir computing approach. *Physical review letters*, 120(2):024102, 2018.

[75] Jaideep Pathak, Zhixin Lu, Brian R Hunt, Michelle Girvan, and Edward Ott. Using machine learning to replicate chaotic attractors and calculate lyapunov exponents from data. *Chaos: An Interdisciplinary Journal of Nonlinear Science*, 27(12):121102, 2017.

[76] RA Petersen and MM Samet. On the preferred mode of jet instability. *Journal of Fluid Mechanics*, 194:153–173, 1988.

[77] J Peterson and Y Bayazitoglu. Measurements of velocity and turbulence in vertical axisymmetric isothermal and buoyant jets. 1992.

[78] SB Pope. An explanation of the turbulent round-jet/plane-jet anomaly. *AIAA journal*, 16(3):279–281, 1978.

[79] BR Ramaprian and MS Chandrasekhara. Lda measurements in plane turbulent jets. 1985.

[80] L Raynal, J-L Harion, M Favre-Marinet, and G Binder. The oscillatory instability of plane variable-density jets. *Physics of Fluids*, 8(4):993–1006, 1996.

[81] Maxime Roger, Pedro JM Coelho, and Carlos B da Silva. Large eddy simulations of turbulent heated jets. In *Proceedings of CHT-12. ICHMT International Symposium on Advances in Computational Heat Transfer*. Begel House Inc., 2012.

[82] S Russ and PJ Strykowski. Turbulent structure and entrainment in heated jets: The effect of initial conditions. *Physics of Fluids A: Fluid Dynamics*, 5(12):3216–3225, 1993.

[83] Baris A Sen and Suresh Menon. Turbulent premixed flame modeling using artificial neural networks based chemical kinetics. *Proceedings of the Combustion Institute*, 32(1):1605–1611, 2009.

[84] Aamir Shabbir and William K George. Experiments on a round turbulent buoyant plume. *Journal of Fluid Mechanics*, 275:1–32, 1994.

[85] Noah Shofer. *Reservoir computing: Memory, nonlinearity, and spatial observers*. PhD thesis, Reed College, 2018.

[86] Mark D Skowronski and John G Harris. Automatic speech recognition using a predictive echo state network classifier. *Neural networks*, 20(3):414–423, 2007.

[87] EJ Smith, J Mi, GJ Nathan, and BB Dally. Preliminary examination of a" round jet initial condition anomaly" for the k-ε turbulence model. In *15th Australasian Fluid Mechanics Conference*, pages 1–4. Citeseer, 2004.

[88] Charles G Speziale. Turbulence modeling for time-dependent rans and vles: a review. *AIAA journal*, 36(2):173–184, 1998.

[89] KR Sreenivasan, S Raghu, and D Kyle. Absolute instability in variable density round jets. *Experiments in Fluids*, 7(5):309–317, 1989.

[90] SA Stanley and S Sarkar. Influence of nozzle conditions and discrete forcing on turbulent planar jets. *AIAA journal*, 38(9):1615–1623, 2000.

[91] Hitoshi Suto, Koji Matsubara, Mutsuo Kobayashi, and Yoshiaki Kaneko. Large eddy simulation of flow and scalar transport in a round jet. *Heat Transfer—Asian Re-*

search: Co-sponsored by the Society of Chemical Engineers of Japan and the Heat Transfer Division of ASME, 33(3):175–188, 2004.

[92] Gouhei Tanaka, Toshiyuki Yamane, Jean Benoit Héroux, Ryosho Nakane, Naoki Kanazawa, Seiji Takeda, Hidetoshi Numata, Daiju Nakano, and Akira Hirose. Recent advances in physical reservoir computing: A review. *Neural Networks*, 115:100–123, 2019.

[93] Artur Tyliszczak and Andrzej Boguslawski. Les of the jet in low mach variable density conditions. In *Direct and Large-Eddy Simulation VI*, pages 575–582. Springer, 2006.

[94] David Verstraeten, Benjamin Schrauwen, Michiel d'Haene, and Dirk Stroobandt. An experimental unification of reservoir computing methods. *Neural networks*, 20(3):391–403, 2007.

[95] Pantelis R Vlachas, Wonmin Byeon, Zhong Y Wan, Themistoklis P Sapsis, and Petros Koumoutsakos. Data-driven forecasting of high-dimensional chaotic systems with long short-term memory networks. *Proceedings of the Royal Society A: Mathematical, Physical and Engineering Sciences*, 474(2213):20170844, 2018.

[96] Ping Wang, Jochen Fröhlich, Vittorio Michelassi, and Wolfgang Rodi. Large-eddy simulation of variable-density turbulent axisymmetric jets. *International Journal of Heat and Fluid Flow*, 29(3):654–664, 2008.

[97] Alexander Wikner, Jaideep Pathak, Brian Hunt, Michelle Girvan, Troy Arcomano, Istvan Szunyogh, Andrew Pomerance, and Edward Ott. Combining machine learning with knowledge-based modeling for scalable forecasting and subgrid-scale closure of large, complex, spatiotemporal systems. *Chaos: An Interdisciplinary Journal of Nonlinear Science*, 30(5):053111, 2020.

[98] David Wilcox. A half century historical review of the k-omega model. In *29th Aerospace Sciences Meeting*, page 615, 1991.

[99] Jonathan W Woolley, PK Agarwal, and John Baker. Modeling and prediction of chaotic systems with artificial neural networks. *International journal for numerical methods in fluids*, 63(8):989–1004, 2010.

[100] Heng Xiao and Paola Cinnella. Quantification of model uncertainty in rans simulations: A review. *Progress in Aerospace Sciences*, 108:1–31, 2019.

[101] Bayya Yegnanarayana. *Artificial neural networks*. PHI Learning Pvt. Ltd., 2009.

[102] Zeng Yuhong and Huai Wenxin. Application of artificial neural network to predict the friction factor of open channel flow. *Communications in Nonlinear Science and*

Numerical Simulation, 14(5):2373–2378, 2009.

[103] Siti Nurul Akmal Yusuf, Yutaka Asako, Nor Azwadi Che Sidik, Saiful Bahri Mohamed, and Wan Mohd Arif Aziz Japar. A short review on rans turbulence models. *CFD Letters*, 12(11):83–96, 2020.

[104] KBMQ Zaman and AKMF Hussain. Turbulence suppression in free shear flows by controlled excitation. In *13th Fluid and PlasmaDynamics Conference*, page 1338, 1981.

[105] Chun Zhang, Junjie Jiang, Shi-Xian Qu, and Ying-Cheng Lai. Predicting phase and sensing phase coherence in chaotic systems with machine learning. *Chaos: An Interdisciplinary Journal of Nonlinear Science*, 30(8):083114, 2020.

[106] G Peter Zhang. Time series forecasting using a hybrid arima and neural network model. *Neurocomputing*, 50:159–175, 2003.

[107] Yang Zhiyin. Large-eddy simulation: Past, present and the future. *Chinese journal of Aeronautics*, 28(1):11–24, 2015.

[108] X Zhou, KH Luo, and JJR Williams. Study of density effects in turbulent buoyant jets using large-eddy simulation. *Theoretical and Computational Fluid Dynamics*, 15(2):95–120, 2001.

.